NTIA Report 97-337

Field Strength Measurements of DGPS and FAA Beacons in the 285- to 325-kHz Band

J.R. Hoffman
J.J. Lemmon
R.L. Ketchum

U.S. DEPARTMENT OF COMMERCE
William M. Daley, Secretary

Larry Irving, Assistant Secretary
for Communications and Information

June 1997

PRODUCT DISCLAIMER

Certain commercial equipment, instruments, or materials are identified in this paper to specify adequately the technical aspects of the reported results. In no case does such identification imply recommendation or endorsement by the National Telecommunications and Information Administration, nor does it imply that the material or equipment identified is the best available for the purpose.

All Maps in this report were produced with MapExpert™ software from DeLorne Mapping.

CONTENTS

Page

FIGURES

Page

FIGURES (Cont'd)

Page

FIGURES (Cont'd)

Page

FIGURES (Cont'd)

Page

TABLES

Page

FIELD STRENGTH MEASUREMENTS OF DGPS AND FAA BEACONS IN THE 285- TO 325-kHz BAND

J. Randy Hoffman, John J. Lemmon, Ronald L. Ketchum [1]

Signal strength measurements in the 285- to 325-kHz band were conducted on eight U.S. Coast Guard differential global positioning system beacons along the Gulf and West Coast, and on a Federal Aviation Administration beacon in Bennett, Colorado. Data were acquired continually en route between sites and tagged with geographical position. Field strength of each individual signal was plotted against distance from the transmitter. Cumulative distributions and histograms of deviation from the least squares fit were also plotted. Results of the measurements were used as model inputs and to compare results to model predictions.

Key words: differential GPS (DGPS); global positioning system (GPS); signal strength measurements; U.S. Coast Guard beacon; FAA beacon; propagation models

1. PURPOSE

The purpose of this study was to determine absolute differential global positioning system (DGPS) signal strengths at various distances from eight different U.S. Coast Guard beacons transmitting DGPS signals and to measure signal strength at various distances from a Federal Aviation Administration (FAA) beacon located in the same frequency band.[2] Four of the measured DGPS beacons are located along the Gulf Coast and four are on the West Coast. The measured FAA beacon is located in Bennett, Colorado, east of Denver. Each of the transmitters are described in Table 1. Results of the measurements are used to provide model inputs and to compare results to actual model predictions.

2. STRATEGY

Measurements in the southern region were conducted by driving along the Gulf Coast between Corpus Christi, Texas and Mobile, Alabama. On the first day, the measurement van was driven to the U.S. Coast Guard station at Aransas Pass, Texas (see Figure 1). Starting approximately 17 km from the transmitter, signal strength measurements (304-kHz band only) were performed

---

[1] The authors are with the Institute for Telecommunication Sciences, National Telecommunications and Information Administration, U.S. Department of Commerce, Boulder, CO 80303

[2] This effort was sponsored by the Federal Highway Administration, Department of Transportation.

Table 1. Beacon Characteristics

Location	Frequency (kHz)	Antenna	Transfer Rate (bps)	Latitude (N)	Longitude (W)
Aransas Pass, Texas	304	PA90B	100	27° 50'18''	97°03'33''
English Turn, Louisiana	293	PA90B	200	29°52'44''	89°56'31''
Galveston, Texas	296	PA90B	100	29°19'45''	94°44'10''
Mobile Point, Alabama	300	150 ft Tower	100	30°13'38''	88°01'24''
Pigeon Point, California	287	PA90B	100	37°10'55''	122°23'35''
Point Blunt, California	310	PA90B	200	37°51'12''	122°25'04''
Cape Mendocino, California	292	PA90B	100	40°26'29''	124°23'56''
Fort Stevens, Oregon	287	PA90B	100	46°12'18''	123°57'21''
Bennett, Colorado	321	Unknown	N/A	39°47'31''	104°26'03''

as the measurement vehicle was driven along the southwest edge of the bay; through Corpus Christi, circling around the bay to the north (see Figure 2). On the second day, measurements were conducted between Corpus Christi, Texas and Lafayette, Louisiana while traveling along Highways 77, 59, and Interstate 10. All four U.S. Coast Guard transmitters were monitored continuously (except for a short break taken as the vehicle came in close proximity to the Galveston, Texas site). The vehicle was driven to the town of Galveston via Highway 6 and then transported by ferry across the bay. Measurements resumed on the opposite shore. Data were acquired to within 5 km of the Galveston transmitter. For the remainder of the distance between Galveston, Texas and Lafayette, Louisiana, data were acquired at nighttime. On the third day, measurements were conducted continuously on all four Gulf State transmitters as the vehicle traveled between Lafayette, Louisiana and Mobile, Alabama along Interstate 10. En route, the measurement vehicle came within 11 km of the English Turn, Louisiana transmitter (see

Figure 3). On the fourth day, measurements were conducted near the Mobile Point transmitter (300-kHz band only) as the vehicle was driven to the transmitter site from the west side of the bay. Data were acquired to within 10 km of the transmitter (see Figures 4 and 5).

On the West Coast, signal strength measurements were conducted on each of the four DGPS transmitters by driving the following routes: Data were acquired on the DGPS signal from the transmitter at Cape Mendocino, California while driving north from Santa Rosa, California along Highway 101 within 12 km of the transmitter and continuing north to Crescent City, California. From there, the measurement vehicle was driven along Highway 199 to Grants Pass, Oregon. Cape Mendocino is located approximately halfway between Santa Rosa and Grants Pass along Highway 1 (see Figure 6). Data were acquired on the DGPS signal from

Figure 1. Transmitter at Aransas Pass, Texas.

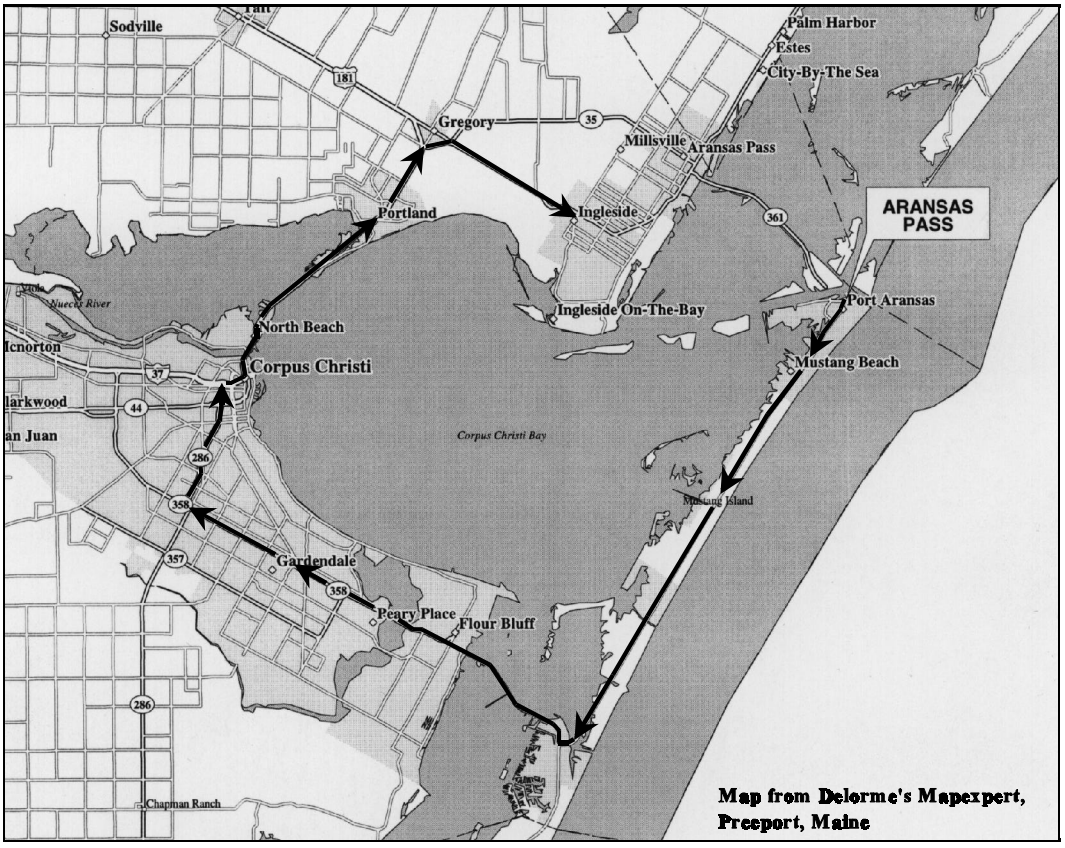

Figure 2. Measurement route at Aransas Pass, Texas.

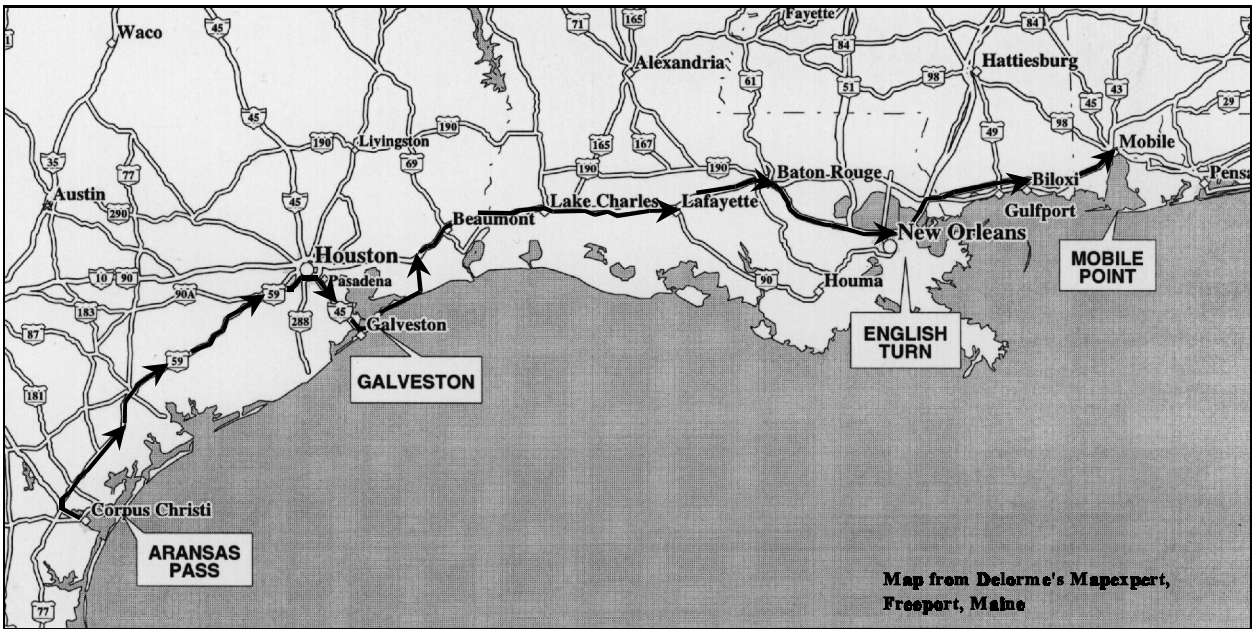

Figure 3. Measurement route between Aransas Pass, Texas and Mobile Point, Alabama.

the transmitter at Fort Stevens, Oregon starting at a distance of 10 km from the transmitter on Highway 30, traveling along the Columbia River east to The Dalles, Oregon (see Figure 7). Both nighttime and daytime data were acquired on the Pigeon Point, California and Point Blunt, California transmitters. Pigeon Point is located approximately 45 km north of Santa Cruz, California along Highway 1, and Point Blunt is located on Angel Island in the San Francisco Bay. Nighttime data were acquired by driving south from Willits, California along Highway 101 to the Golden Gate Bridge and continuing along Highway 1 to Santa Cruz. Daytime data were acquired by starting 6 km south of the Pigeon Point transmitter traveling south to Santa Cruz, across the coastal mountains on Highway 17, north on the eastern border of the bay along Interstate 680, east along Interstate 80, over the Sierra Nevada Mountains, and past Reno, Nevada (see Figure 6).

Figure 4. Transmitter at Mobile Point, Alabama.

Data on the FAA beacon at Bennett, Colorado were acquired on two different routes. The first route started at the transmitter traveling west along Interstate 70 over

Figure 5. Measurement route at Mobile Point, Alabama.

the Rocky Mountains to Grand Junction, Colorado. The second route started at the transmitter traveling west along Interstate 70 to Interstate 25 and then north to approximately 50 km north of Cheyenne, Wyoming (see Figure 8). The primary reason for measuring the signal strength on the FAA beacon was to examine the propagation characteristics through the Rocky Mountains west of Denver. The data collected on the second route was used to compare propagation characteristics for flat terrain in the same approximate vicinity.

3. MEASUREMENT SYSTEM

The measurement system (see Figure 9) consists of a receiving antenna, low pass filter, amplifier, spectrum analyzer, global positioning system (GPS)/dead-reckoning (DR) receiver, and a computer. The antenna was calibrated for antenna-correction factors at 2-kHz intervals between 285 kHz and 325 kHz (see Appendix C). The low pass filter serves to filter out all frequencies

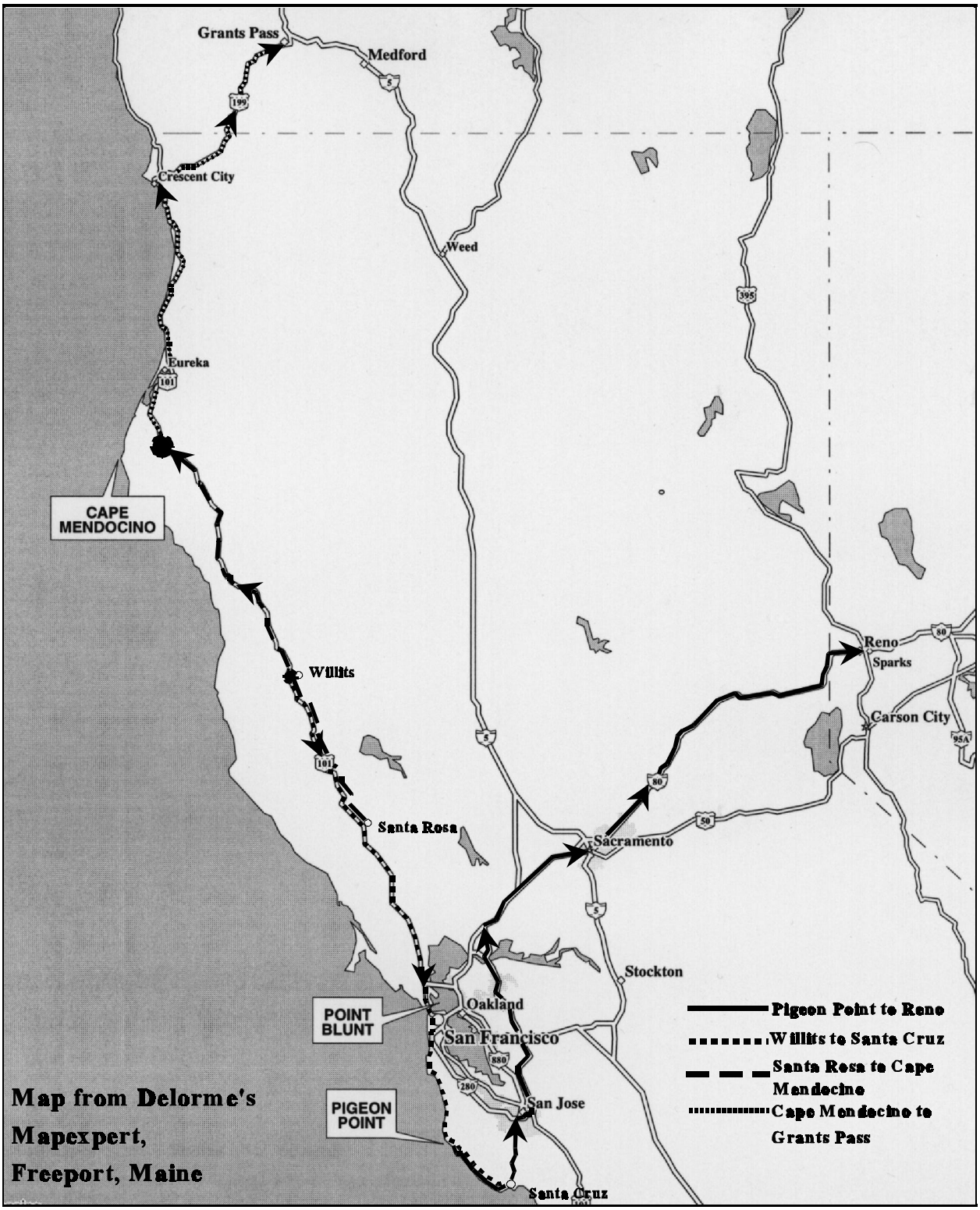

Figure 6. Measurement routes for Cape Mendocino, California; Point Blunt, California; and Pigeon Point, California.

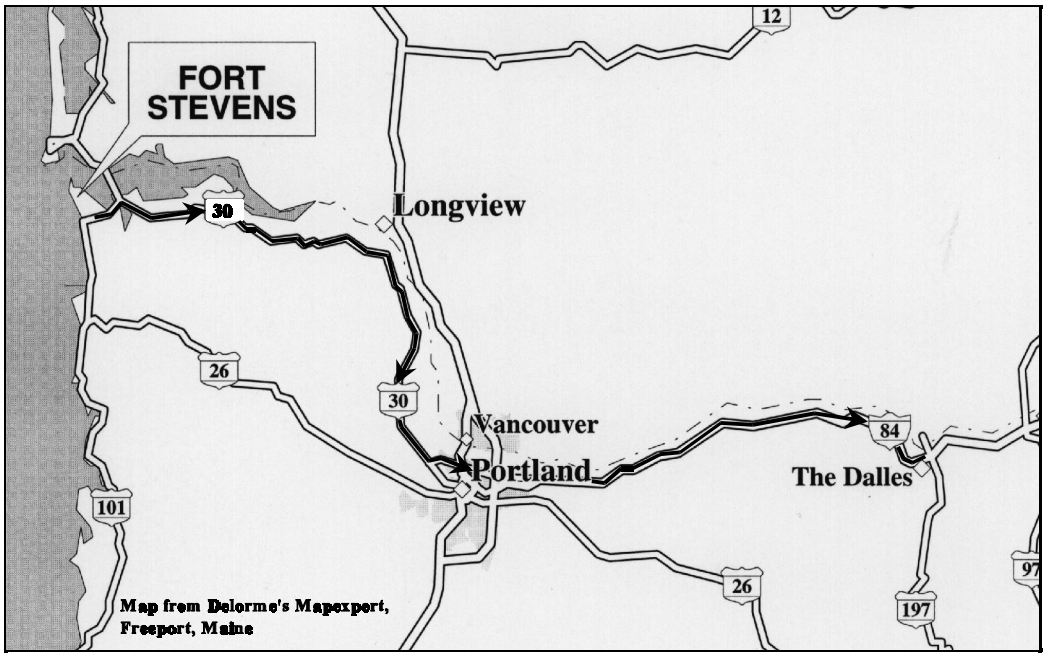

Figure 7. Measurement route at Fort Stevens, Oregon.

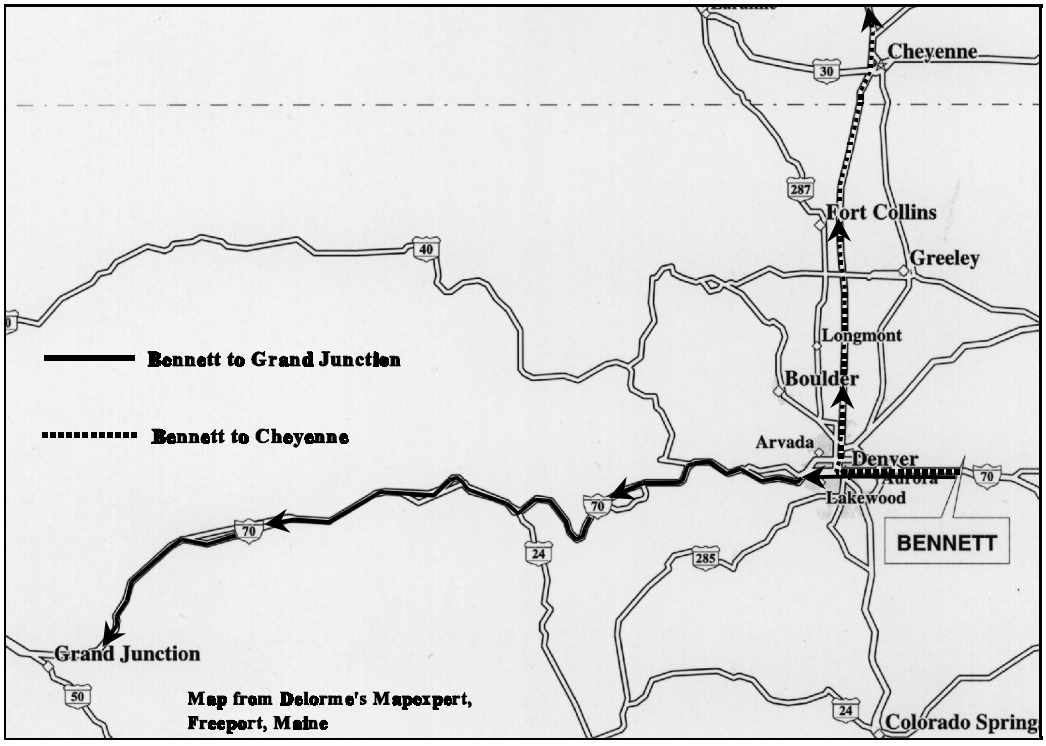

Figure 8. Measurement route for the FAA beacon.

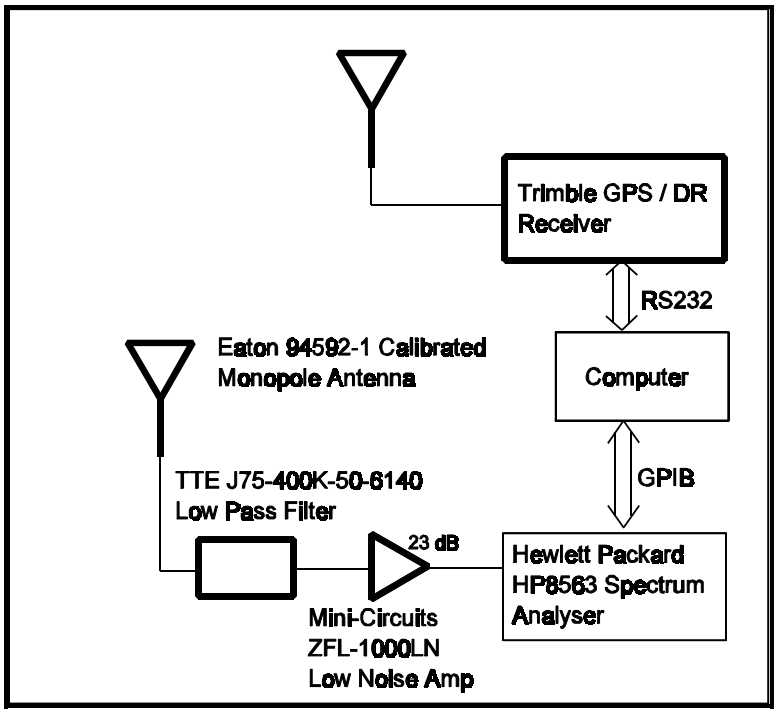

Figure 9. Block diagram of the measurement system.

above 400 kHz, particularly the AM broadcast bands. The computer is used to control the spectrum analyzer, download raw data, gather GPS information, and perform various computations. The overall gain of the system between the output of the antenna and the measured output of the spectrum analyser is approximately 24 dB. The noise figure of the system is 9.6 dB, giving a sensitivity of 7.85 dB μV/m for a bandwidth of 300 Hz (see Appendix B). The GPS receiver has a dead-reckoning system such that, if satellite lock is lost, the proper coordinate information is maintained.

4. MEASUREMENT PROCEDURE

The computer controlled the acquisition of data using GPIB and RS232 commands sent to the spectrum analyzer and GPS receiver, respectively. Data also were downloaded via GPIB and RS232. Both noise and DGPS signal strength data were acquired.

Prior to acquiring data on the DGPS signal, the power of the noise was determined by making measurements 500 Hz offset from the DGPS carrier frequency. The noise was measured to determine if the signal, as a whole, could be detected against the noise background. The purpose of measuring noise was not to determine environmental noise, even though, in many cases, this may have been the primary source of noise. Three types of measurement procedures were used: type 1 in the Gulf States, type 2 for Cape Mendocino, California, and type 3 for all the remaining

beacons along the West Coast and Colorado. The three measurement types are described in Table 2. Note that for type 2 noise measurements, the spectrum analyser was set to zero span and swept in time as opposed to the other two types which were swept in frequency. To avoid measuring power from the adjacent DGPS signal itself, the resolution bandwidth of type 1 and 2 measurements was kept relatively small. For noise measurements, a single sweep was performed; after which, the mean, the standard deviation, and the peak noise power were determined from 601 data points evenly spaced across the sweep. Type 2 and 3 measurements also collected 50 samples evenly spaced across the 601 data points of the sweep. Because the filters on the HP8563 spectrum analyzer are gaussian with a gentle roll-off and the measured signals are only 500 Hz offset from the locations of the noise measurements, type 2 measurements resulted in an upward bias due to the contribution of power by the adjacent signal. Therefore, the measurement technique was changed to a type 3 noise measurement shortly after completing data acquisition on the Cape Mendocino beacon. For all three techniques, there was an upward bias when the noise measurements were conducted in close physical proximity to the transmitter because the signal could contribute significantly to the power received within the bandwidth. This, again, is because the filters in the HP8563 spectrum analyzer have a gentle roll-off and the measured signals are only 500 Hz offset from the location of the noise measurements.

The DGPS signal strength was measured by performing 50 separate sweeps of a 500-Hz span spaced between 1-5 s apart. After each sweep, the signal power was determined and recorded in the data file. For a type 1 acquisition, the peak power over the entire span was determined and recorded. For type 2 and 3 acquisitions, the power was determined at the DGPS center frequency. The power determination at center frequency is believed to be better since the determination of peak power over an entire span may cause a slight upward bias from spurious noise spikes. Based on the antenna-correction factor and the known frequency, the signal field strength was calculated as described in Appendix A. With each sweep, a data string from the GPS was downloaded and placed in the file to mark the location of the acquisition. Each of the four parameters (frequency, power, field strength, and GPS coordinate string) were recorded for each of the 50 sweeps. The DGPS transmission rates are either 100 or 200 bps with minimum shift keyed modulation (MSK). For MSK, 99% of the power is contained within a bandwidth equal to 1.17 times the bit rate. Therefore, the resolution bandwidth of the spectrum analyzer was set at 300 Hz when acquiring DGPS signal strength data. When more than one band was monitored, the system acquired noise data and DGPS signal strength data (on the 50 sweeps for a particular frequency band) and then performed the same operations on each of the successive bands. After completing the data acquisition on each of the bands, the entire process was repeated continuously.

Two calibration procedures were performed before acquiring data. The first procedure was used to determine the total gain between the output of the antenna and the measured power determined by the spectrum analyzer. This gain was subtracted from the measured power to determine the power at the output of the antenna. The procedure amounted to putting a signal of known power into the cable which was normally connected to the antenna, and then the power was measured on the spectrum analyzer. The difference between the known power and the measured power is

Table 2. Measurement Procedures for Noise and DGPS Signals

Noise Measurements			
Parameters	**Type 1**	**Type 2**	**Type 3**
Locations	Gulf States	Cape Mendocino, California	Remaining beacons on West Coast and the FAA beacon in Colorado
Span of Spectrum Analyser	500 Hz	Zero Span	200 Hz
Resolution Bandwidth	30 Hz	300 Hz	10 Hz
Sweep Type	Frequency	Time	Frequency
Sweep Time	360 ms	700 ms	350 ms
Parameters Measured	Mean, standard deviation, & peak	Mean, standard deviation, & peak	Mean, standard deviation, & peak
Additional Data Acquired	None	50 samples across the sweep	50 samples across the sweep
DGPS Signal Measurements			
Parameters	**Type 1**	**Type 2**	**Type 3**
Location	Gulf States	Cape Mendocino, California	Remaining beacons on West Coast and the FAA beacon in Colorado
Span of Spectrum Analyser	500 Hz	500 Hz	500 Hz
Power Measured	Over the entire frequency span	At the DGPS signal center frequency	At the DGPS signal center frequency
Resolution Bandwidth	300 Hz	300 Hz	300 Hz

the gain of the system, which in this case is approximately 24 dB.

The second calibration procedure was used to determine any differences in antenna characteristics between those measured in a laboratory (during which the antenna-correction factor was determined) and the characteristics of the antenna when placed on the measurement van. First, the antenna was placed at the center of a 1.3-m round backplane which, in turn, was mounted on a tripod approximately 1 m above ground. This backplane configuration was used to simulate the measurement conditions in the laboratory. The power of a known transmitted signal (such as a DGPS signal) was measured. Then the antenna was mounted on the measurement van and the power of the same signal was measured at eight different azimuth orientations by the van (approximately 45° apart). Results showed essentially no difference between the two different antenna mounts and among the eight different azimuth orientations.

5. DATA PROCESSING

Data processing consisted of ordering the data and placing the results in an ASCII file for plotting. Since the distance between a specific transmitter and the receiver does not necessarily monotonically increase or decrease with each successive data point, the data was processed by ordering the data according to distance. This was performed for each of the nine transmitters listed in Table 1. After ordering the data, several parameters were written to an ASCII file: distance, DGPS field strength, and noise field strength for an equivalent 300-Hz bandwidth.

6. ANALYSIS

Results showing the signal strength as a function of distance from each of the transmitter sites can be seen in Figures 10-22 (pp. 18-24). The noise is represented as an equivalent field strength for a 300-Hz bandwidth. An additional 10 and 15 dB are added to noise data acquired at 30- and 10-Hz bandwidths, respectively.[3] The signal strength and equivalent average noise (for a 300-Hz bandwidth) are plotted against the distance on the abscissa. For the Gulf Coast measurements, the average noise was determined from successive groups of 50 data points. In other words, the

[3] The equivalent noise power P_e expressed in terms of a given bandwidth B_e is given by

$$P_e = P_m + 10 \log_{10} \frac{B_e}{B_m}$$

where P_m is the power measured at bandwidth B_m.

first point on the plot represents the average of the first group of 50 data points, the second point on the plot represents the average of the second group of 50 data points, and so on. For all West Coast and FAA beacon measurements, each point on the plot represents a moving average of the data. This was accomplished by determining the average of the previous 50 data points for each successive data point. The least squares fit for signal strength as a linear function of the log base 10 of the distance also was determined for each of the transmitter sites shown in Table 3.

As a check of the system calibrations, expected signal levels at a specified distance from the transmitter can be compared against measured values. At the Galveston site, the U.S. Coast Guard reported an antenna efficiency of 15-20% with a signal input to the antenna of 1 kW. This is consistent with the approximate measured signal level of 80 dB μV/m at 10 km (see Appendix D).

Cumulative distribution curves and histogram plots for deviation from the least squares fit are shown in Figures 23-42 (pp. 25-34). The same data points used to calculate the least squares fit were used for these plots. Negative numbers represent signal strength occurring below the least squares fit. The upper and lower bounds for the 99% confidence interval are included on each of the cumulative distribution curves [1]. The numerical values for the 80% and 99% confidence interval are shown in Table 4.

Separate plots and statistical summaries were generated for the different approaches to the Cape Mendocino transmitter. Analysis in which all data were grouped together for this transmitter showed a bimodal distribution related to the direction of approach. This is because the terrain is significantly different when approaching the transmitter from the south or north. South of the transmitter, the terrain is characterized by rolling hills separated by relatively flat regions. North of the transmitter, there are cliffs, heavy forests, deep ravines, and mountainous areas.

7. MEASUREMENT RESULTS

When plotted against the log of the distance, most of the DGPS signal data appear relatively linear with a roll-off of 20 dB per decade. Deviations from this linearity appear in several cases. Aransas Pass and Mobile Point data both show higher than expected signal levels between 300 and 500 km (see Figures 10 and 13). The cause of this is probably due to excess noise. Both the Pigeon Point and Point Blunt daytime data show patterns of deviation that are similar (see Figures 14 and 16). There are two regions of signal attenuation, both of which are located physically in areas of rough terrain. The first dip coincides with crossing the coastal mountain range between Santa Cruz and San Jose on Highway 17 (92 km from Point Blunt and 33 km from Pigeon Point). The second dip coincides with crossing the Sierra Nevada mountain range east on Interstate 80 (200 km from Point Blunt and 250 km from Pigeon Point). It is interesting to note that the Sierra Nevada Mountains behave much like an attenuator. As the rough terrain is traversed, the signal strength drops at a much faster rate, but once the relatively flat terrain of Nevada is approached, the signal drops off at approximately the same slope as before. What

Table 3. Y-intercept and Slope of Least Squares Fit

Location	Y-intercept (dB µV/m)	Slope (dB µV/m) / log(km)	Data Points Used
Aransas Pass, Texas	99.35	-20.17	All points < 350 km
Galveston, Texas	100.42	-20.09	All points < 200 km
English Turn, Louisiana	116.44	-26.10	All data points
Mobile Point, Alabama	95.09	-19.05	All points < 350 km
Pigeon Point, California - night	106.02	-27.88	All data points
Point Blunt, California - night	96.91	-23.92	All data points
Cape Mendocino, California - south	138.17	-53.76	All points < 100 km
Cape Mendocino, California - north	123.15	-37.01	All points < 130 km
Fort Stevens, Oregon	100.75	-29.12	All data points
FAA Beacon at Bennett, Colorado, en route to Cheyenne, Wyoming	82.71	-19.05	All data points

appears to be a very strong signal at approximately 400 km from both transmitters is, in actuality, noise from a relatively severe but short-lived spring storm that occurred while crossing the plains of Nevada. This elevated environmental noise was prolonged (lasting several minutes) and was as strong or stronger than the DGPS signals at any time during the measurement; this demonstrated the need to use Type 9 messaging for broadcasting corrections. The Fort Stevens data (see Figure 20) show a relatively wide deviation from a 20 dB per decade roll-off. Much of these data were acquired in areas of rough terrain, rolling hills, and in the gorge of the Columbia River. The FAA beacon data going north to Cheyenne, Wyoming have a narrow deviation from the least squares fit (see Figures 41 and 42) and track very closely to a roll-off of 20 dB per decade (see Figure 21). Data collected on the same signal going west across the Rocky Mountains, however, look quite different (see Figure 22). In this case, the signal shows considerable attenuation when the mountainous terrain was crossed. It is interesting to note that when acquiring data through the Denver area (between 20 and 70 km from the transmitter) the environmental noise was considerably higher. All four of the Gulf Coast beacons show higher

Table 4. Error Bounds on the Sample Cumulative Distributions

Location	Sample Size	Error Bounds (in probability units)	
		80% Confidence	99% Confidence
Aransas Pass, Texas	5018	±0.015	±0.023
Galveston, Texas	2449	±0.022	±0.033
English Turn, Louisiana	6200	±0.014	±0.021
Mobile Point, Alabama	5750	±0.014	±0.021
Pigeon Point, California - night	2749	±0.020	±0.032
Point Blunt, California - night	2658	±0.021	±0.032
Cape Mendocino, California - south	1400	±0.0286	±0.0436
Cape Mendocino, California - north	1500	±0.0276	±0.0421
Fort Stevens, Oregon	4950	±0.015	±0.023
FAA Beacon at Bennett, Colorado	2999	±0.020	±0.030

signal strengths, but this may be due in part to the upward bias caused by picking the peak power across a 500-Hz span (previously mentioned).

Cumulative distributions of the deviation from the least squares fit are relatively consistent among the four different transmitter sites in the Gulf States (see Figures 23-30). There is a 0.98 probability in this case, that the DGPS signal will be greater than 10 dB below the least squares fit. There is a slightly greater spread for nighttime data acquired on Pigeon Point and Point Blunt, and daytime data for Cape Mendocino and Fort Stevens (see Figures 31-40).

8. COMPARISON OF MEASUREMENTS WITH MODELS

As mentioned before, one purpose of carrying out the field strength measurements described in this report is to compare the measurements with the signal strength predictions generated from propagation models. Agreement between the measurements and model predictions serves to validate the models and provides confidence in the use of the models to predict field strengths in regions where measurements have not been performed. Disagreements between the measurements and model predictions can provide insight regarding limitations of the models or indicate a need to modify the models.

Predictions of field strength versus distance have been generated for the four DGPS beacons along the Gulf Coast and for the FAA beacon in Bennett, Colorado. The propagation models are described by Haakinson et al. [2] and references contained therein. The model inputs include transmitter location, frequency, measured field strength at a reference distance, time of day, and ground conductivity. Three types of field strength predictions are possible: smooth earth, which neglects terrain and uses a fixed value of conductivity along the path; smooth earth mixed path, which also neglects terrain but allows the user to construct a path along which the conductivity varies; and irregular terrain, which uses a mixed path and also takes into account terrain features from a terrain database.

Predictions generated from the propagation model were not developed for the beacons on the West Coast. This is because the complicated routes and irregularities in terrain and ground conductivity would make a comparison between predicted and measured field strengths quite tedious, although in principle such a comparison could be made. For the Gulf Coast beacons, the relatively high values of ground conductivity and absence of terrain features result in field strengths (versus distance) that are nearly independent of the direction from the beacon. For this reason, the model predictions could be accurately compared to data measured in multiple directions from the beacon. Because of insignificant variation in terrain and ground conductivity, model predictions were made using the smooth earth model. For the FAA beacon, there are dramatic variations in both terrain and ground conductivity, but the routes were quite simple (essentially due north and due west), so that mixed paths of ground conductivity could be developed for both routes using a conductivity database; model predictions were made using both the smooth earth mixed path and irregular terrain models.

The model predictions and measured values of field strengths versus distance for the four DGPS beacons along the Gulf Coast are shown in Figures 43-46 (pp. 35-36). Values of the measured field strengths and corresponding reference distances, used as model inputs, are listed in Table 5. The values of conductivity that were used are the values at the transmitter location, obtained from a conductivity database. The model predictions were generated for daytime hours, since most of the data were obtained during the day. The model and measurements show good agreement at most distances, although the measured values are somewhat larger than the predicted values at large distances. This could be due to noise, which is expected to have a greater upward bias on the measured field strengths when the signal is weak (greater distances), because the scale is

logarithmic (dB). It also could be due to the fact that the field strength data for these beacons were acquired by recording the peak power over an entire span, as described in Section 4, resulting in an upward bias of the measured signal strengths.

The measured field strengths and model predictions for the FAA beacon are shown in Figures 47-50 (pp. 37-38). Again, measured field strengths that were used as model inputs are listed in Table 5, and the models were used to generate predicted signal strength for daytime hours. Comparisons have been made for both routes that were driven (Bennett, Colorado to Cheyenne, Wyoming and Bennett, Colorado to Grand Junction, Colorado) using both the smooth earth mixed path model and the irregular terrain model; thus, the effects of varying ground conductivity and irregular terrain can be separated. Not surprisingly, both models make similar predictions and are in good agreement with the data for the route from Bennett to Cheyenne, over which the terrain is relatively flat. However, the measured field strengths show considerable attenuation when crossing the Rocky Mountains between Bennett and Grand Junction. This is partly due to the relatively poor ground conductivity in the mountains (rock), as can be seen from the smooth earth mixed path model predictions, which neglect terrain. However, the deviations between this model and the measured field strengths, which are as large as 15 dB or more, indicate that terrain features also play a role in the large propagation losses that were observed in this region. Note that these propagation losses are fairly well described by the irregular terrain model. The magnitude of these deviations was somewhat unexpected, because the effects of terrain features on field strengths are not generally this large at these frequencies. For example, the report by DeMinco [3] contains numerous comparisons of predictions of the smooth earth and irregular terrain models for various path profiles and frequencies; these comparisons do not show deviations as large as 15 dB, although deviations as large as 10 dB do occasionally occur.

To further investigate the effects of irregular terrain, comparisons between the smooth earth and irregular terrain models were made for a path going west from Colorado Springs, Colorado, over the continental divide in the Rocky Mountains, and for a path going northeast from Sacramento, California, into the Sierra Nevada Mountains. In both cases, the differences between the field strength predictions of the two models are not more than 0.1 dB. However, it has been shown by Furutsu et al. [4] that deviations as large as 15 dB or more can, in principle, occur in extremely irregular terrain for certain configurations of the transmitter and receiver.

We conclude that irregular terrain is unlikely to have a significant effect on field strength predictions at these frequencies; however, the effects need to be investigated on a case-by-case basis in extremely irregular terrain. The fact that the model predictions and measured field strengths are generally in good agreement provides confidence in the use of these models.

Table 5. Model Input Parameters

Location	Measured Field Strength (dBμV/m)/ Reference Distance (km)
Aransas Pass, Texas	75/20
Galveston, Texas	80/10
English Turn, Louisiana	80/20
Mobile Point, Alabama	80/10
Bennett, Colorado to Grand Junction, Colorado	66/10
Bennett, Colorado to Cheyenne, Wyoming	66/10

9. CONCLUSIONS

Signal strength measurements were conducted on eight DGPS beacons along the Gulf and West Coast, and an FAA beacon in Colorado. The purpose was to provide model inputs and compare measurement propagation characteristics with model predictions. To the extent that they could be compared, the measured data are in good agreement with the model for most distances. At large distances, the measured values are somewhat larger than the predicted values. The difference is believed to be due to the contribution of noise during measurements.

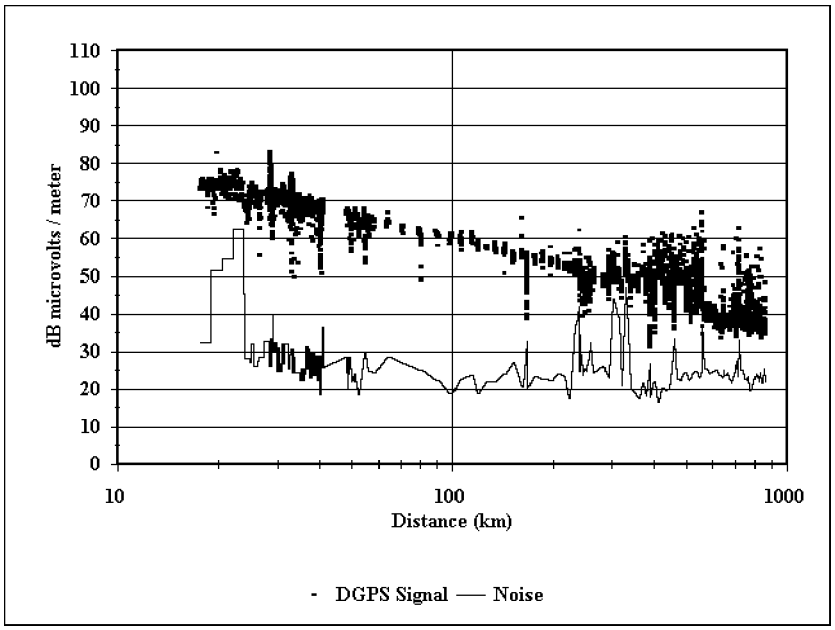

Figure 10. Signal strength vs. distance for the beacon at Aransas Pass, Texas.

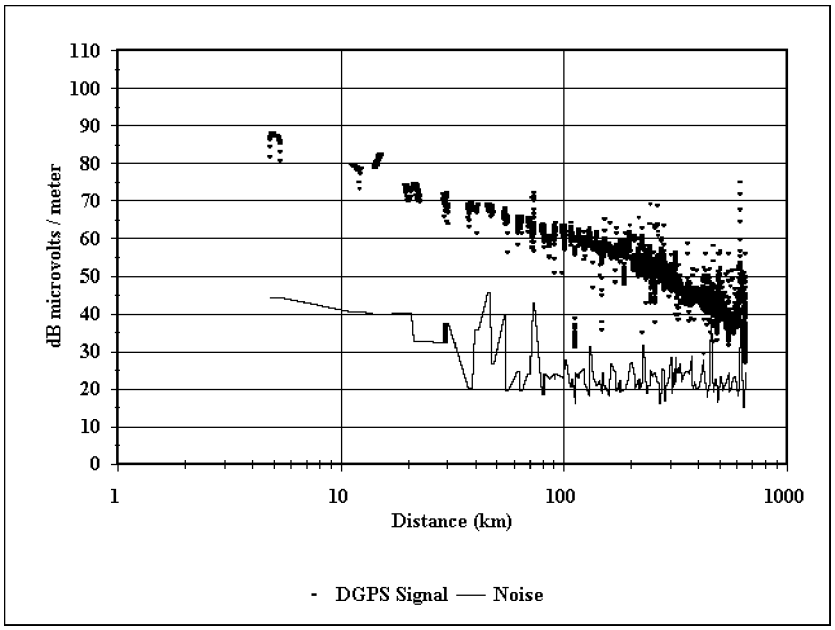

Figure 11. Signal strength vs. distance for the beacon at Galveston, Texas.

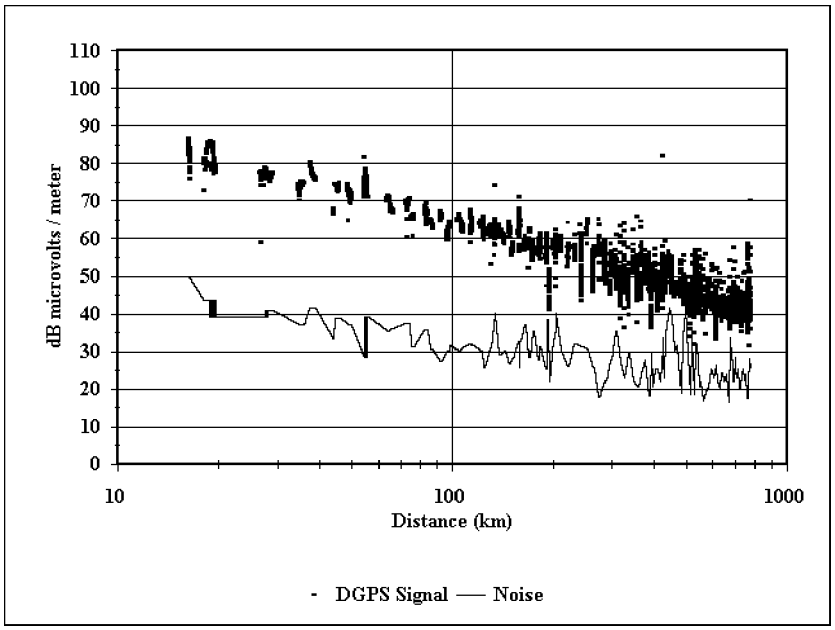

Figure 12. Signal strength vs. distance for the beacon at English Turn, Louisiana.

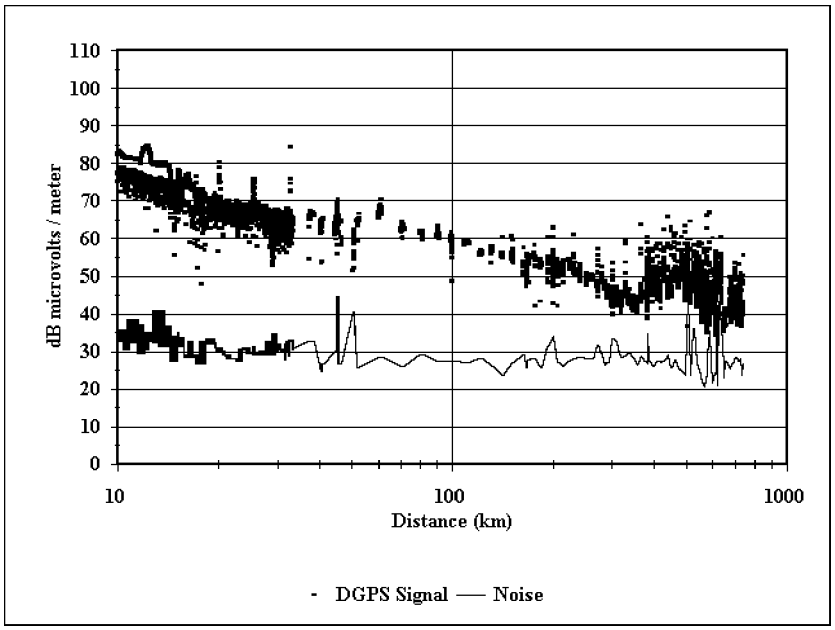

Figure 13. Signal strength vs. distance for the beacon at Mobile Point, Alabama.

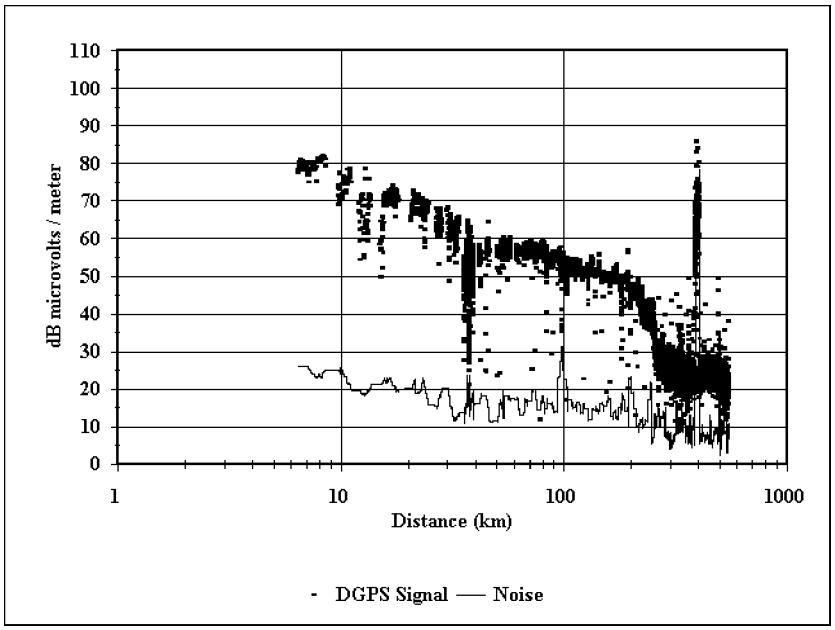

Figure 14. Signal strength vs. distance for the beacon at Pigeon Point, California - daytime measurements.

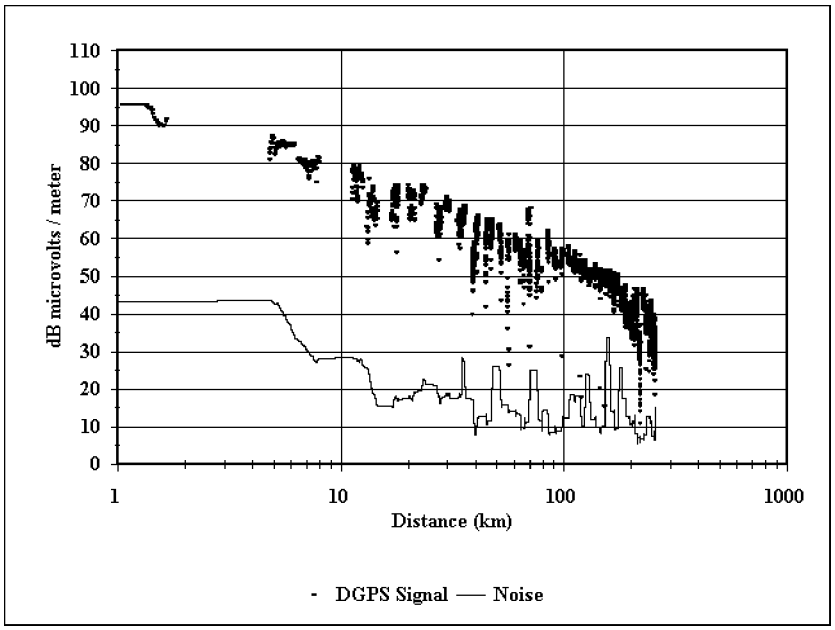

Figure 15. Signal strength vs. distance for the beacon at Pigeon Point, California - nighttime measurements.

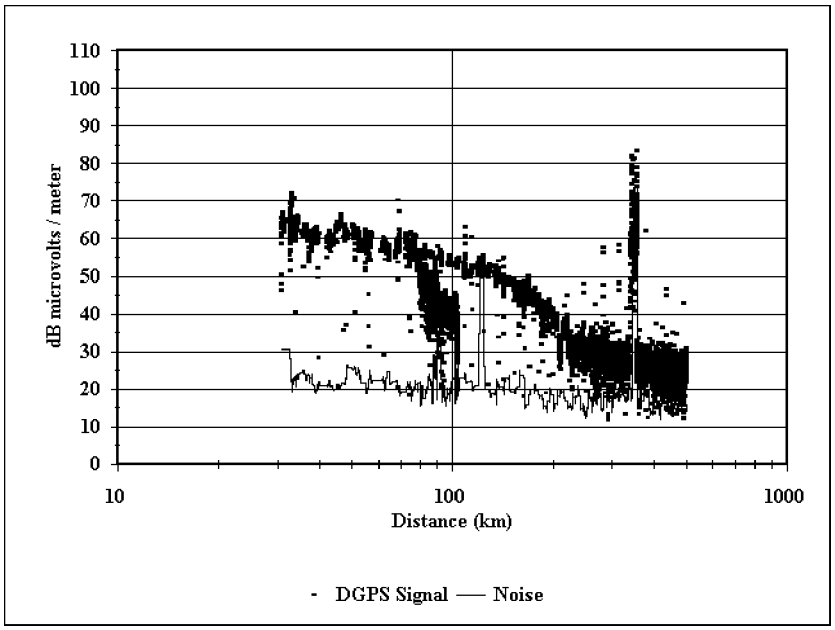

Figure 16. Signal strength vs. distance for the beacon at Point Blunt, California - daytime measurements.

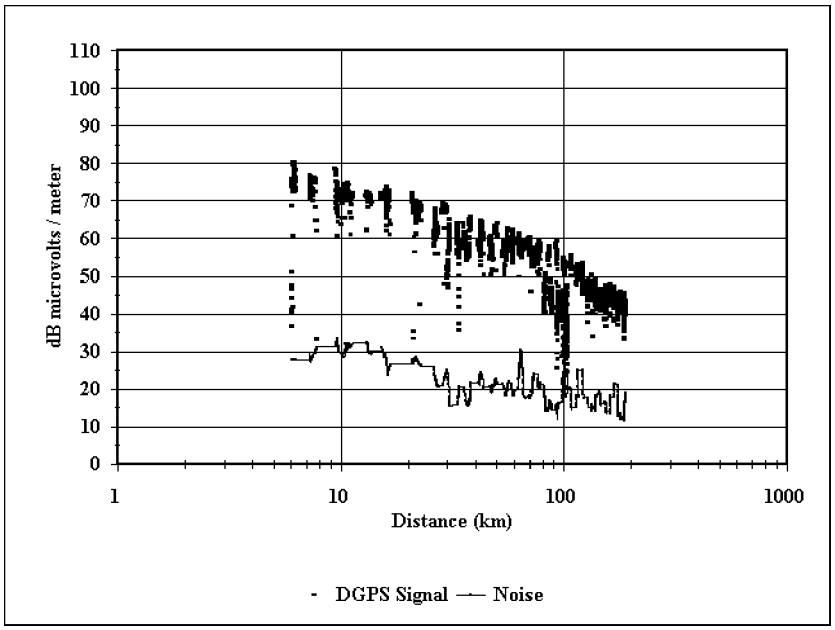

Figure 17. Signal strength vs. distance for the beacon at Point Blunt, California - nighttime measurements.

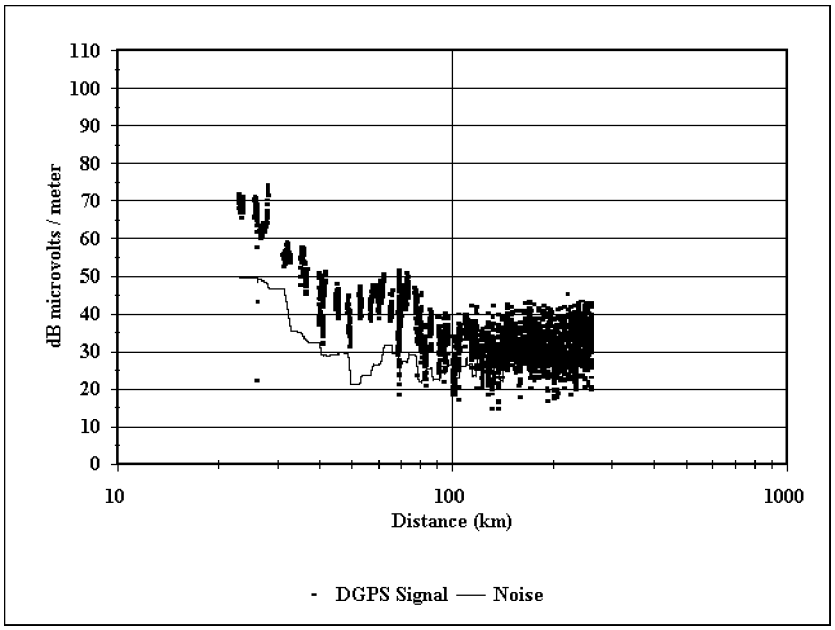

Figure 18. Signal strength vs. distance for the beacon at Cape Mendocino, California - moving north toward the transmitter.

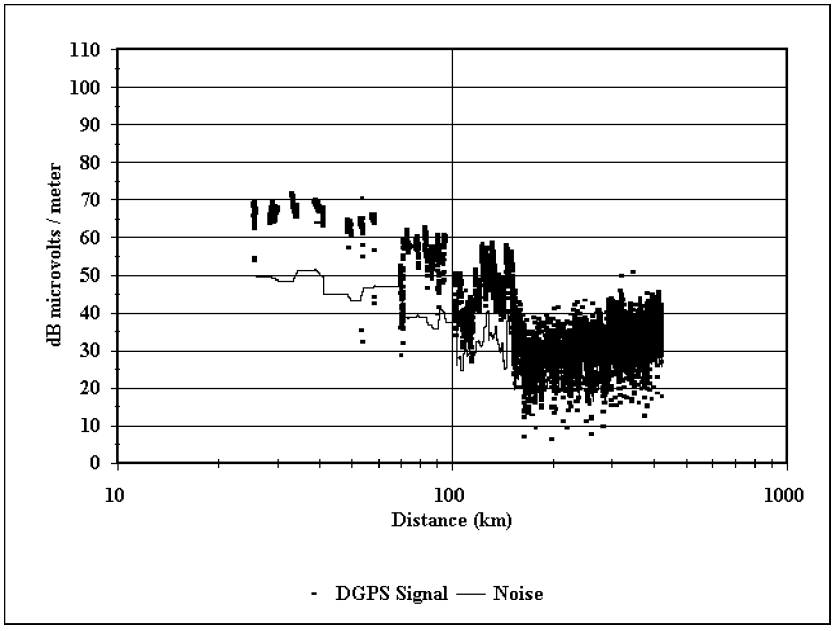

Figure 19. Signal strength vs. distance for the beacon at Cape Mendocino, California - moving north away form the transmitter.

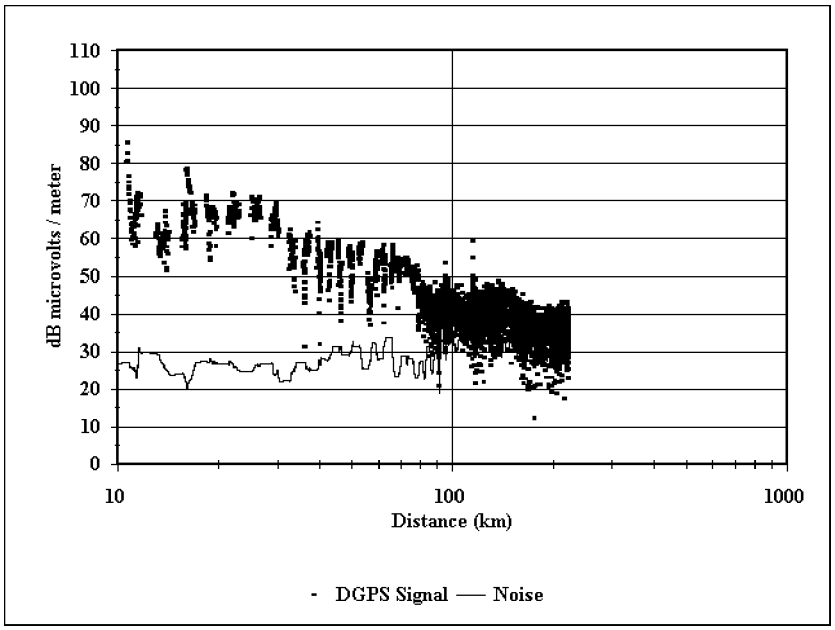

Figure 20. Signal strength vs. distance for the beacon at Fort Stevens, Oregon.

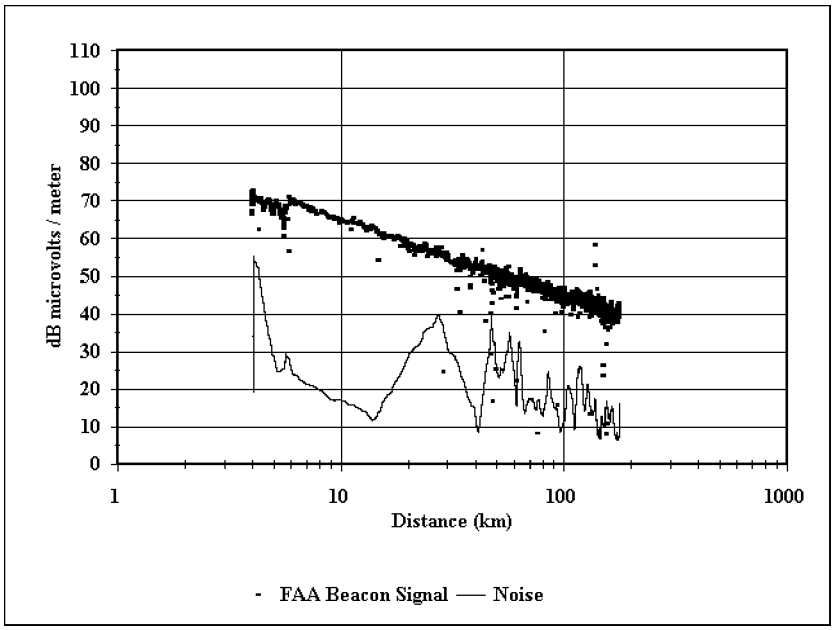

Figure 21. Signal strength vs. distance for the FAA beacon at Bennett, Colorado - en route to Cheyenne, Wyoming.

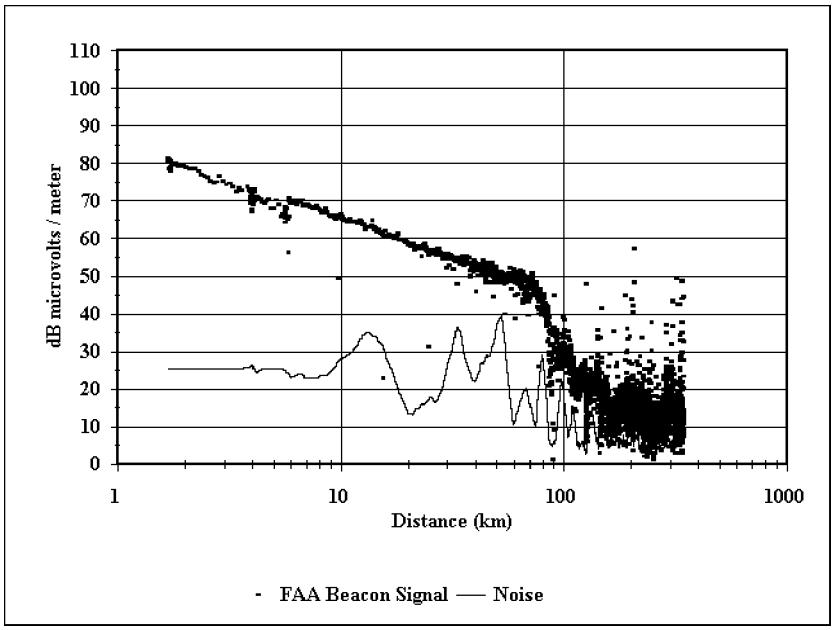

Figure 22. Signal strength vs. distance for the FAA beacon at Bennett, Colorado - en route to Grand Junction, Colorado.

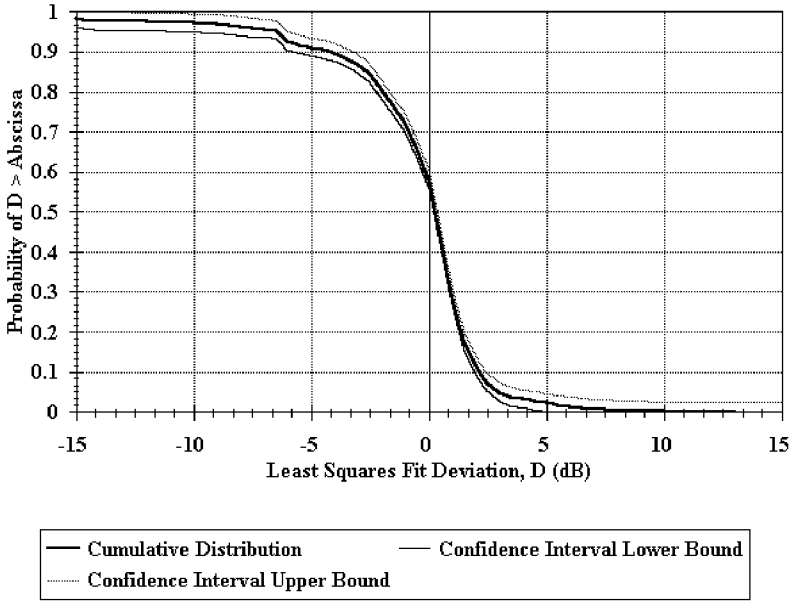

Figure 23. Cumulative distribution of deviation from the least squares fit for Aransas Pass, Texas.

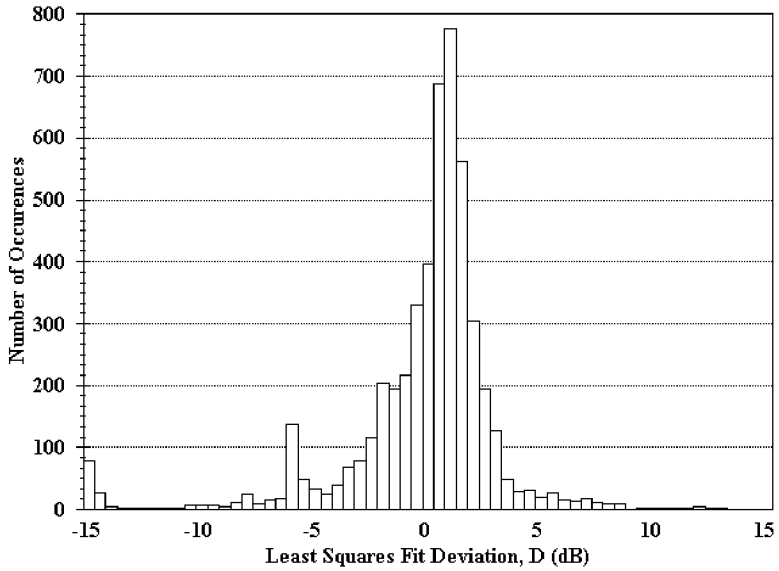

Figure 24. Histogram of deviation from the least squares fit for Aransas Pass, Texas.

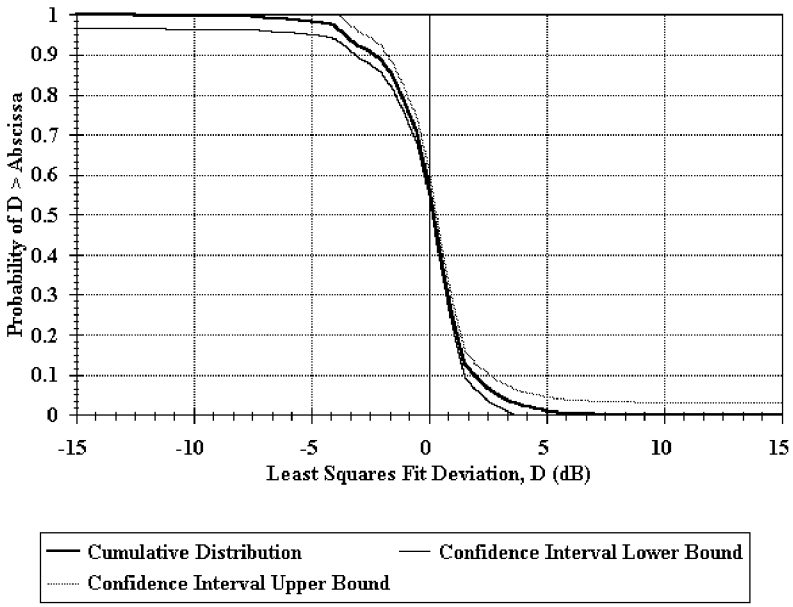

Figure 25. Cumulative distribution of deviation from the least squares fit for Galveston, Texas.

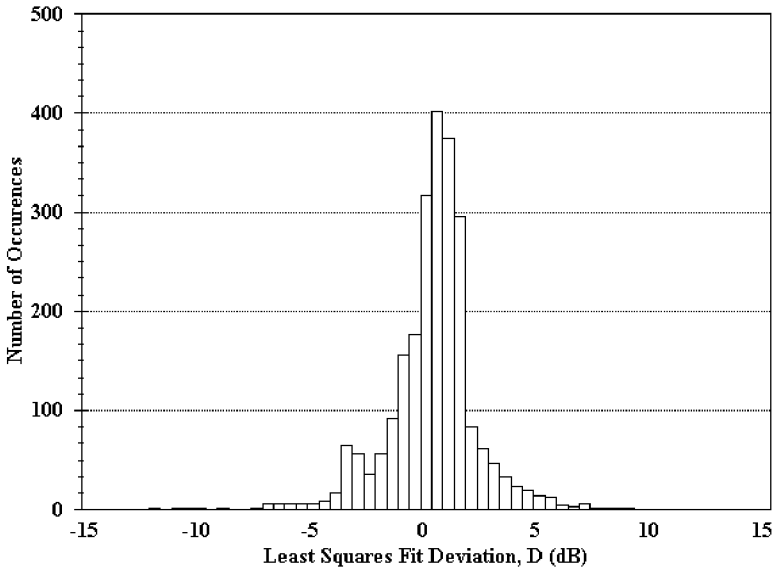

Figure 26. Histogram of deviation from the least squares fit for Galveston, Texas.

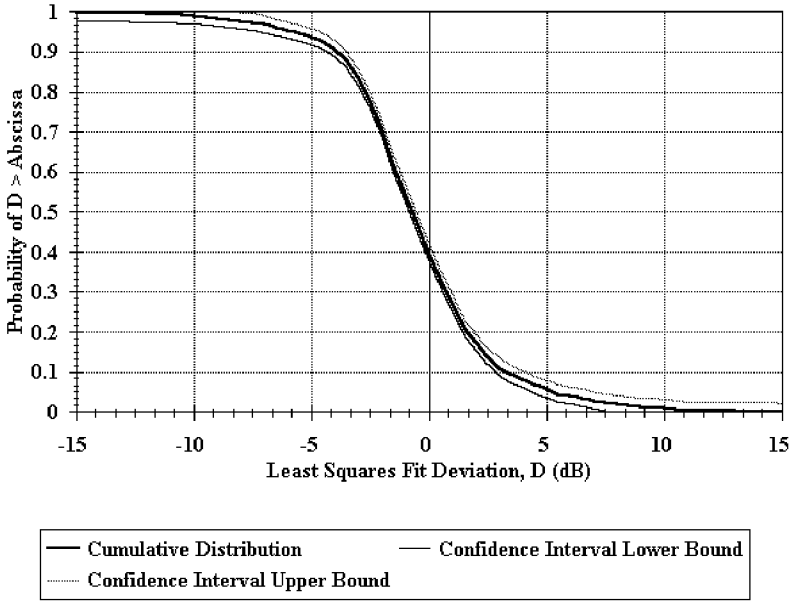

Figure 27. Cumulative distribution of deviation from the least squares fit for English Turn, Louisiana.

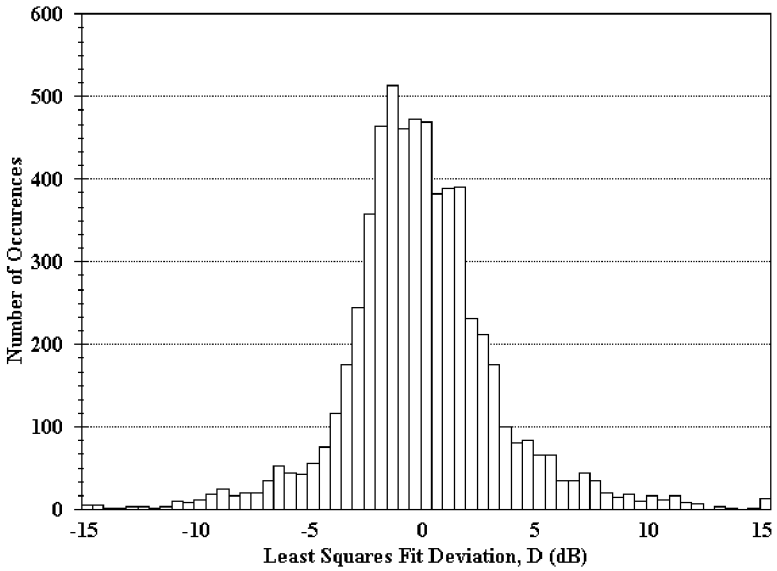

Figure 28. Histogram of deviation from the least squares fit for English Turn, Louisiana.

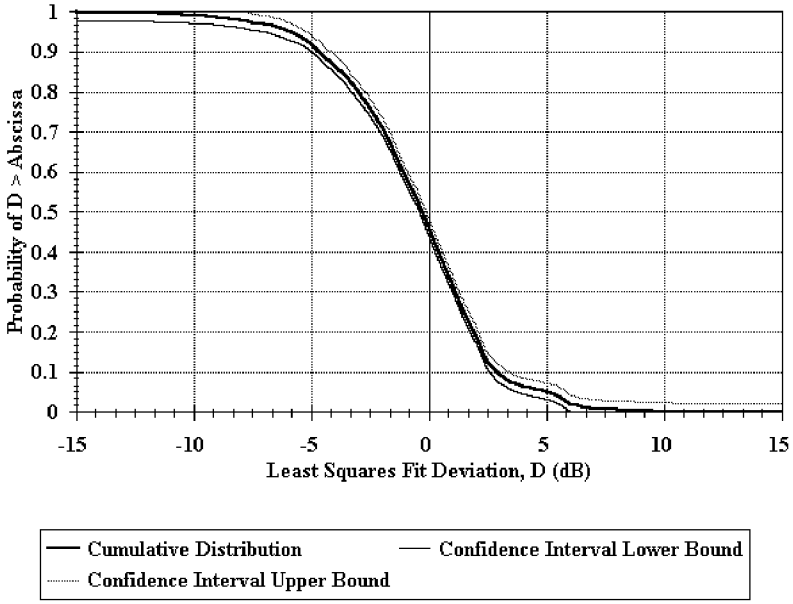

Figure 29. Cumulative distribution of deviation from the least squares fit for Mobile Point, Alabama.

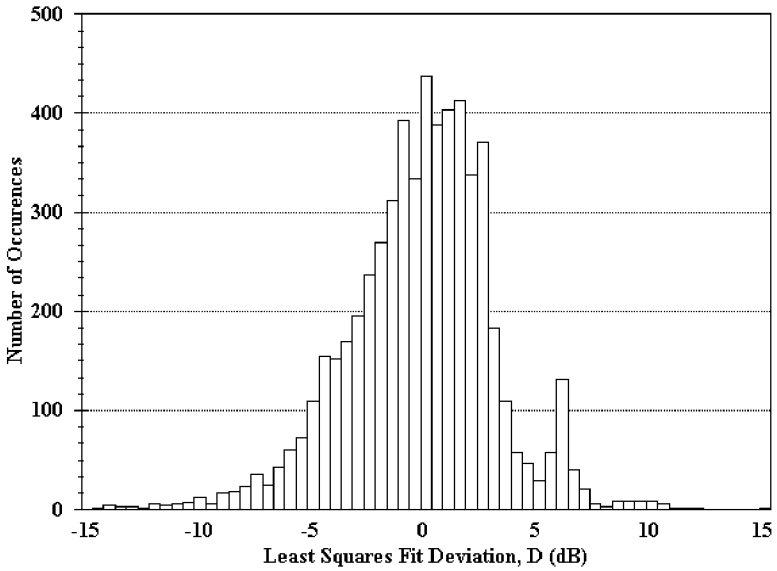

Figure 30. Histogram of deviation from the least squares fit for Mobile Point, Alabama.

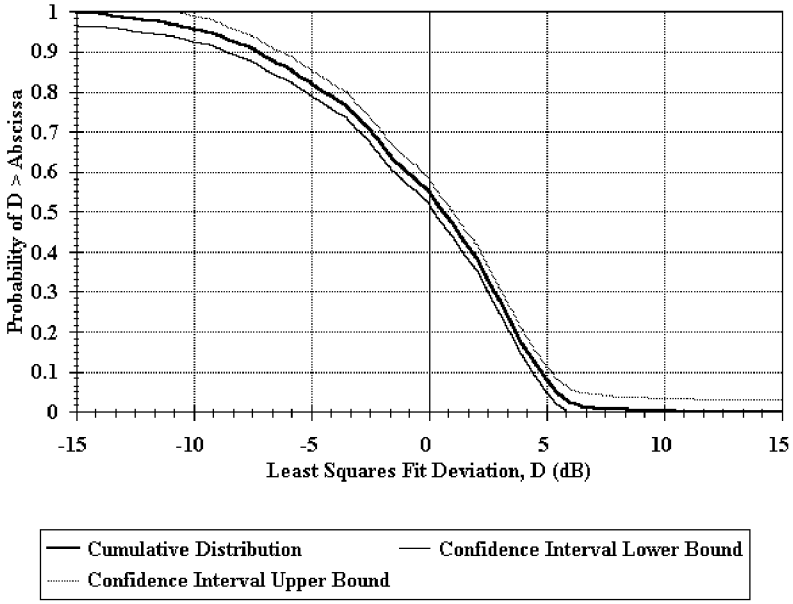

Figure 31. Cumulative distribution of deviation from the least squares fit for Pigeon Point, California - nighttime acquisition.

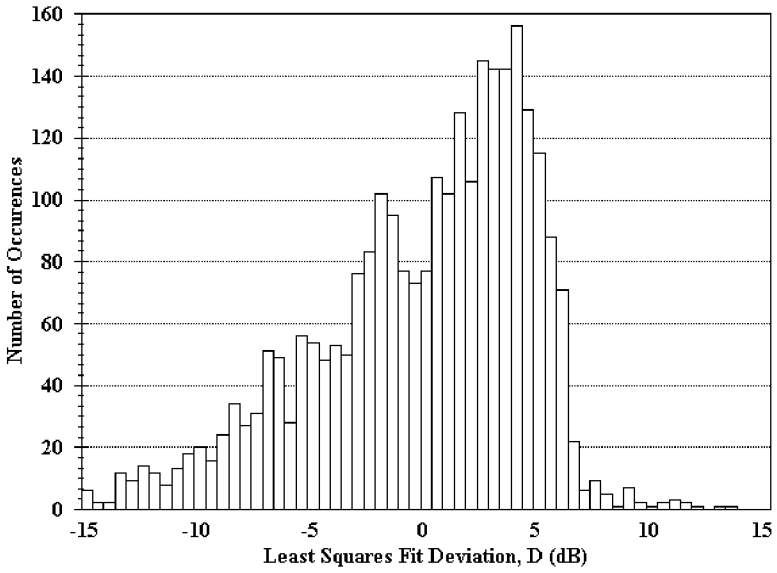

Figure 32. Histogram of deviation from the least squares fit for Pigeon Point, California - nighttime acquisition.

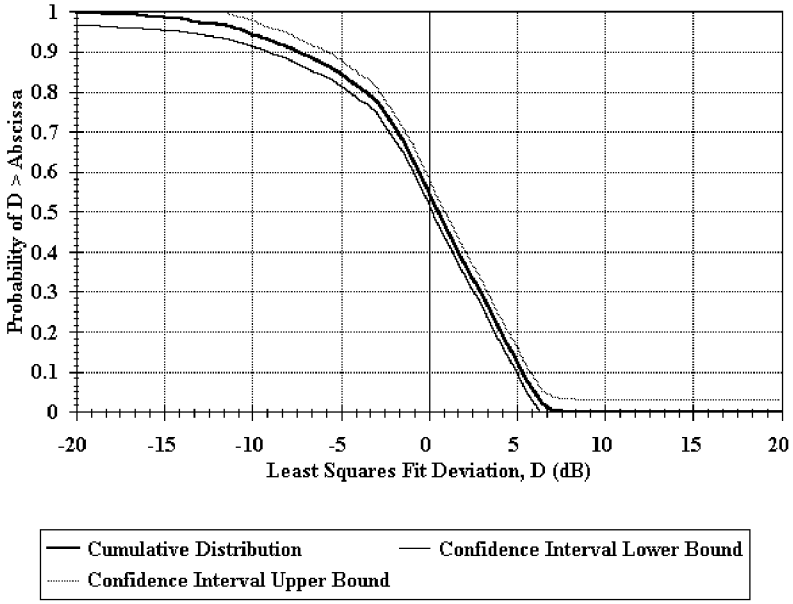

Figure 33. Cumulative distribution of deviation from the least squares fit for Point Blunt, California - nighttime acquisition.

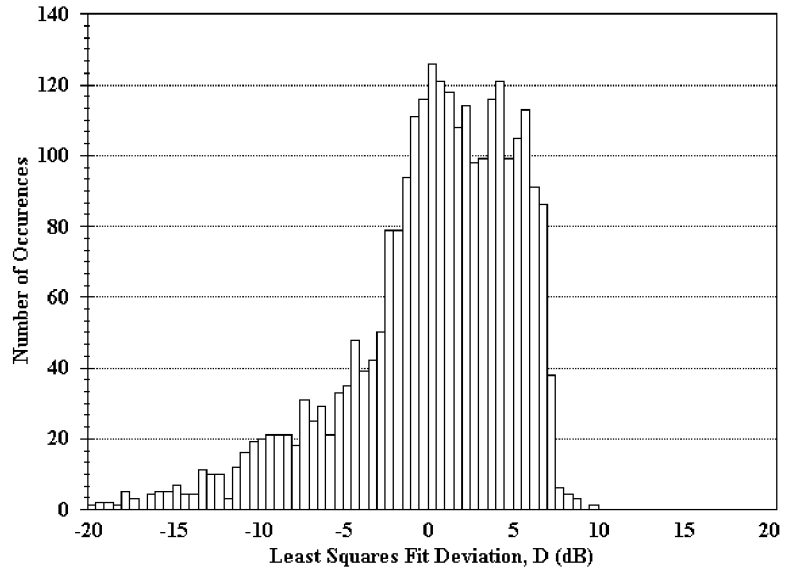

Figure 34. Histogram of deviation from the least squares fit for Point Blunt, California - nighttime acquisition.

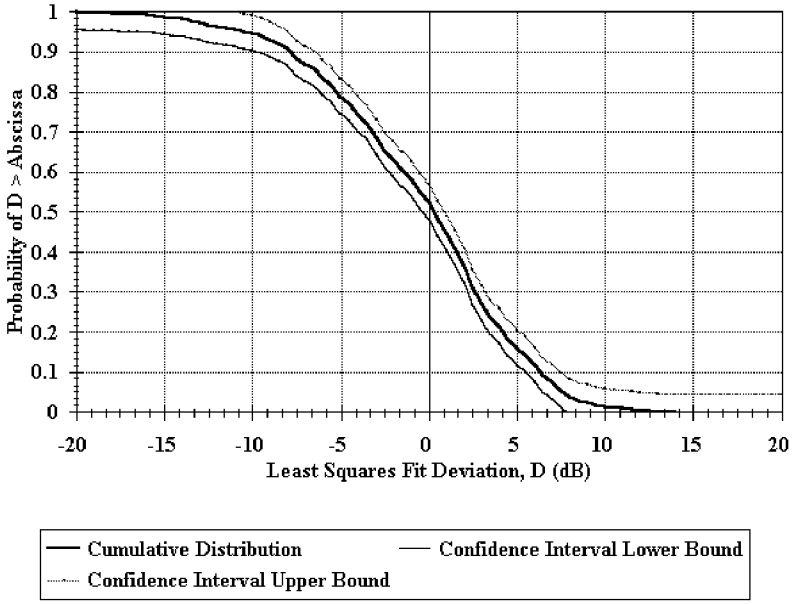

Figure 35. Cumulative distribution of deviation from the least squares fit for Cape Mendocino, California moving north toward the transmitter.

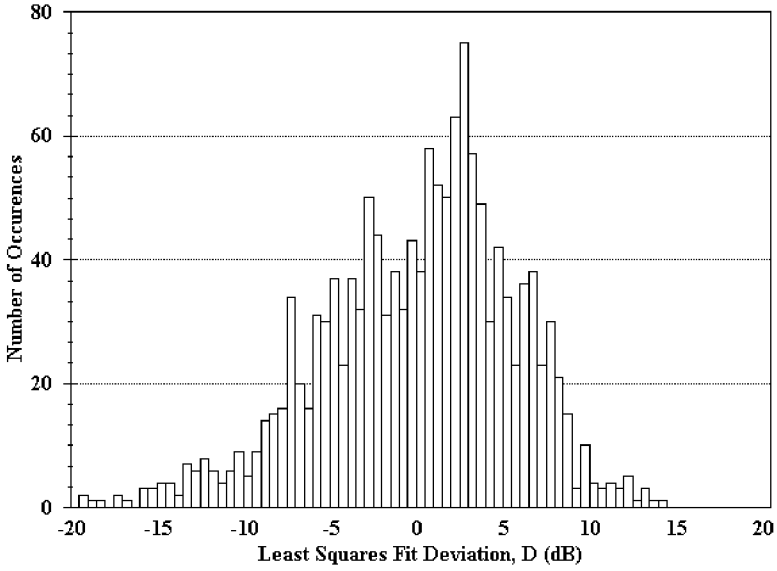

Figure 36. Histogram of deviation from the least squares fit for Cape Mendocino, California moving north toward the transmitter.

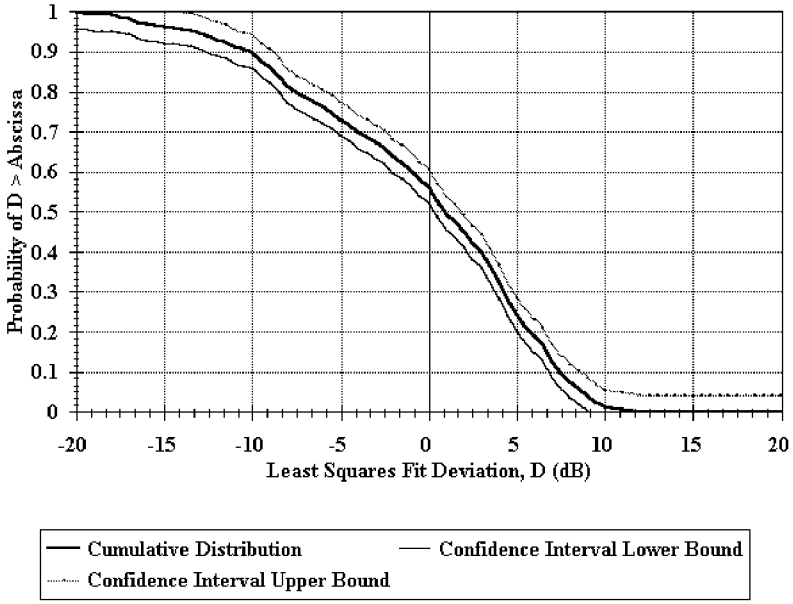

Figure 37. Cumulative distribution of deviation from the least squares fit for Cape Mendocino, California moving north away from the transmitter.

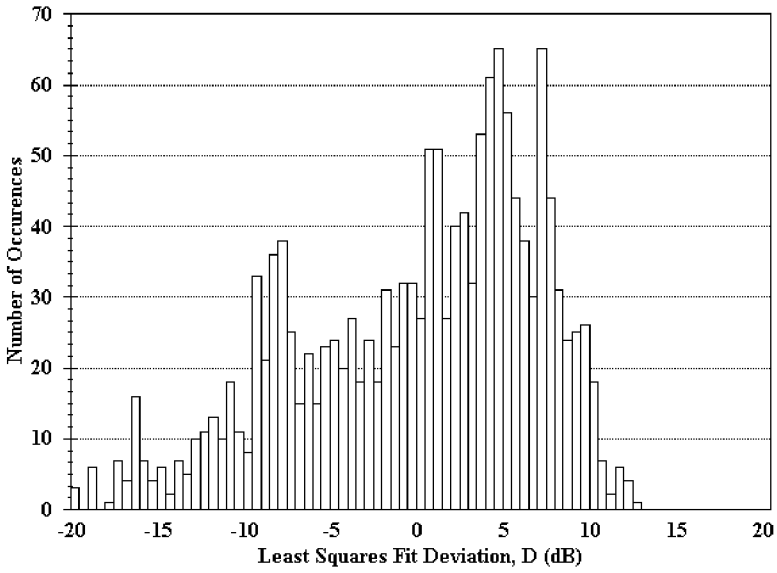

Figure 38. Histogram of deviation from the least squares fit for Cape Mendocino, California moving north away from the transmitter.

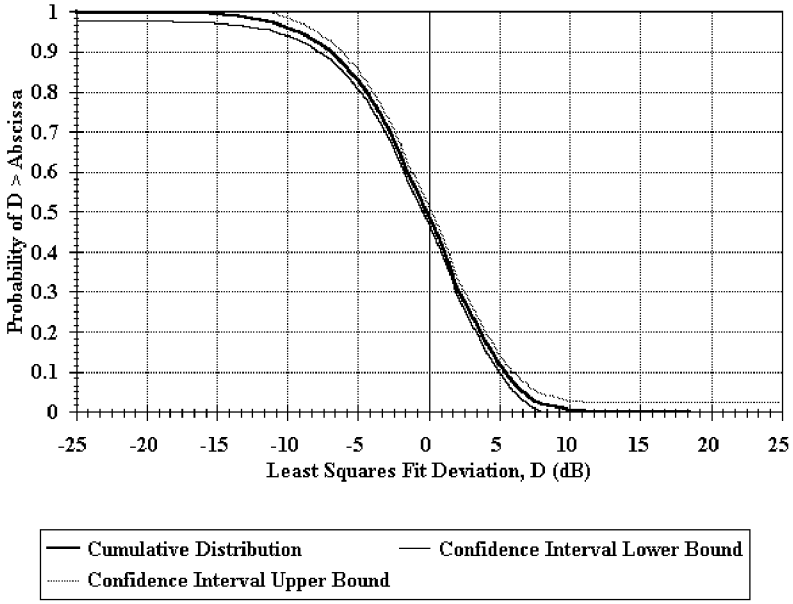

Figure 39. Cumulative distribution of deviation from the least squares fit for Fort Stevens, Oregon.

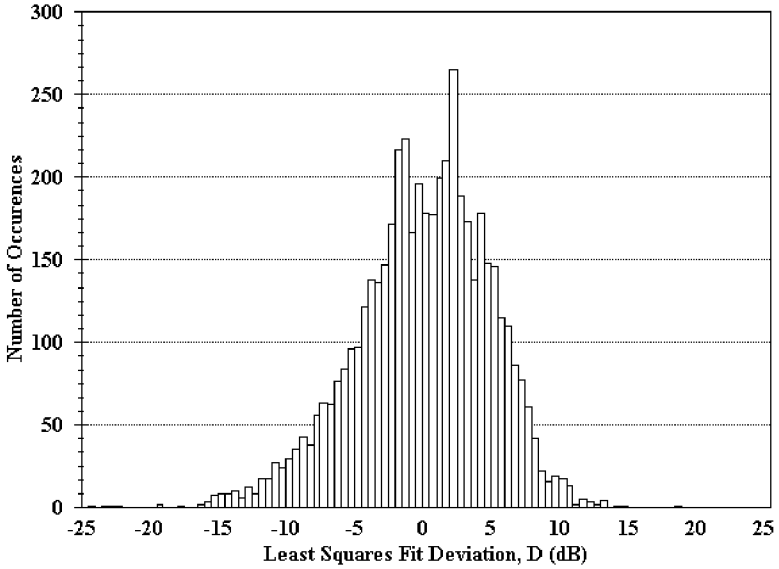

Figure 40. Histogram of deviation from the least squares fit for Fort Stevens, Oregon.

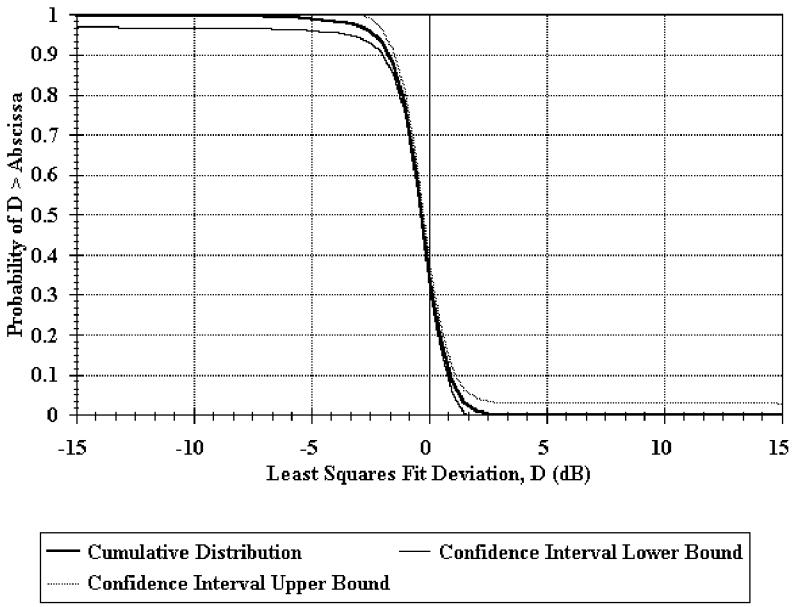

Figure 41. Cumulative distribution of deviation from the least squares fit for the FAA beacon en route to Cheyenne, Wyoming.

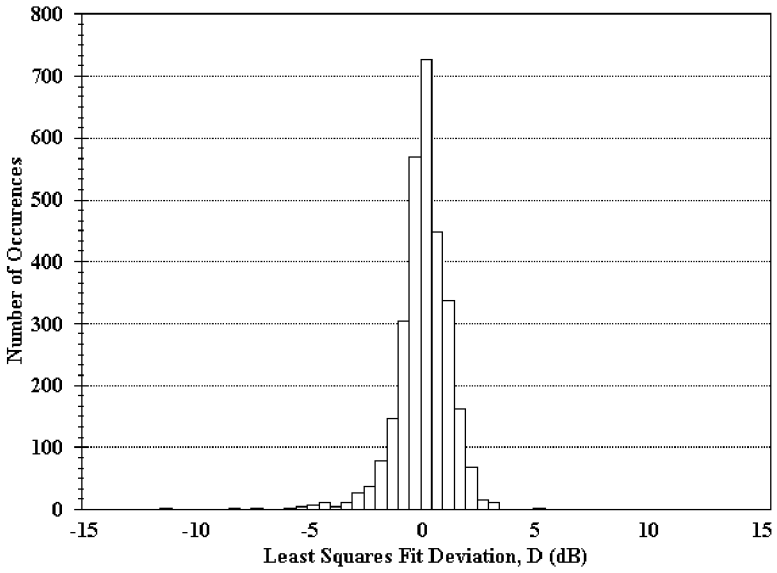

Figure 42. Histogram of deviation from the least squares fit for the FAA beacon en route to Cheyenne, Wyoming.

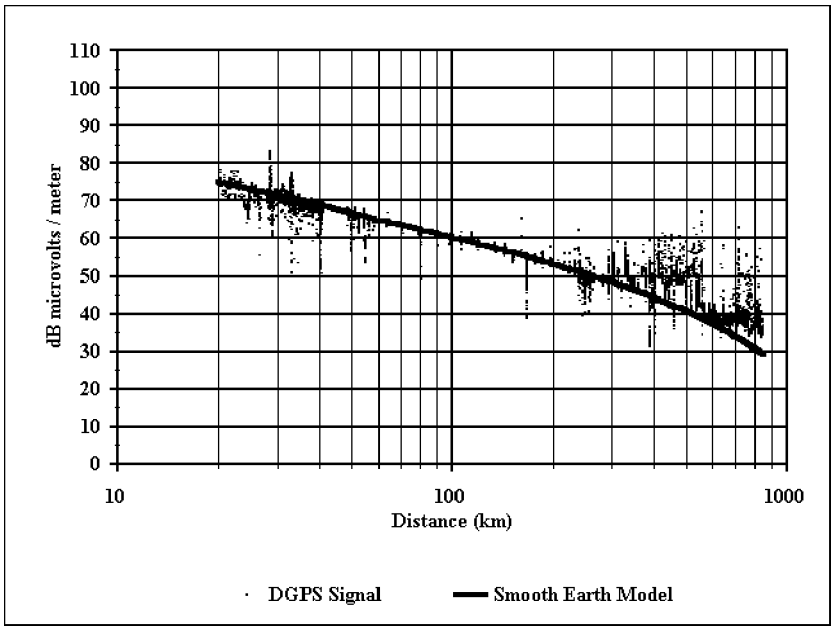

Figure 43. Comparison of measured and predicted field strength vs. distance for Aransas Pass, Texas - smooth earth.

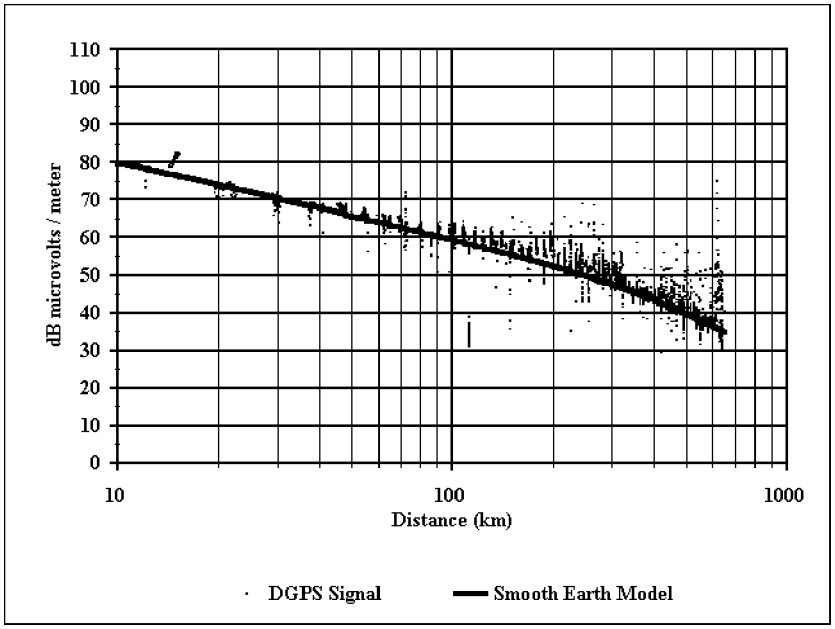

Figure 44. Comparison of measured and predicted field strength vs. distance for Galveston, Texas - smooth earth.

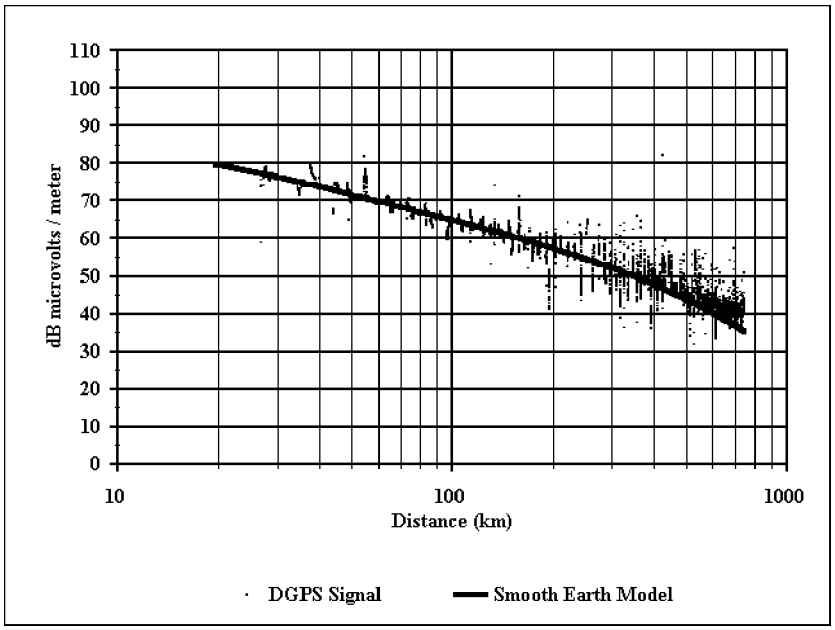

Figure 45. Comparison of measured and predicted field strength vs. distance for English Turn, Louisiana - smooth earth.

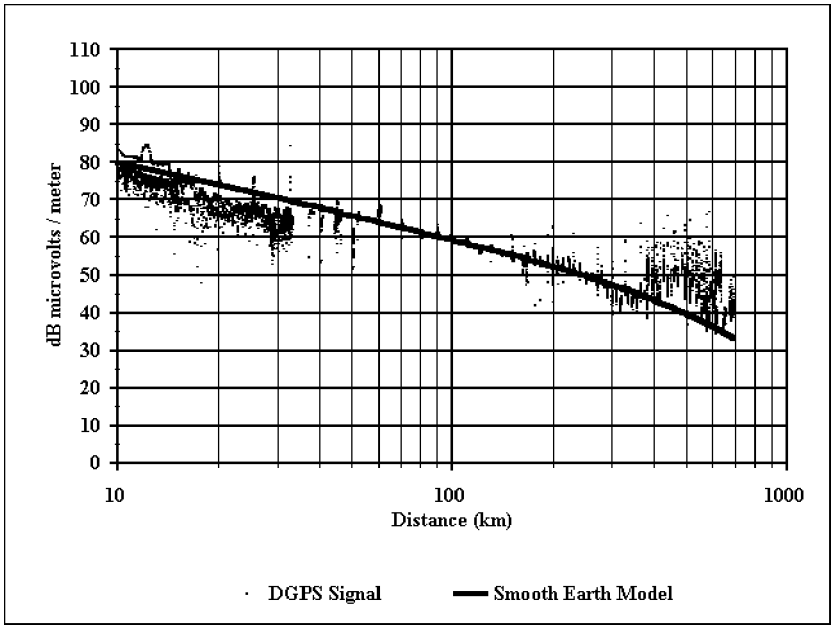

Figure 46. Comparison of measured and predicted field strength vs. distance for Mobile Point, Alabama - smooth earth.

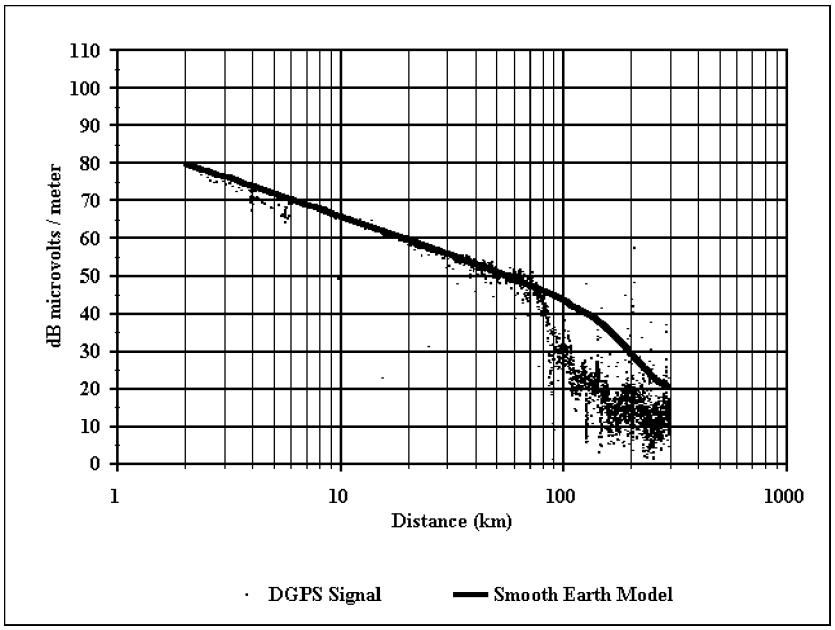

Figure 47. Comparison of measured and predicted field strength vs. distance going west from the FAA beacon at Bennett, Colorado - smooth earth.

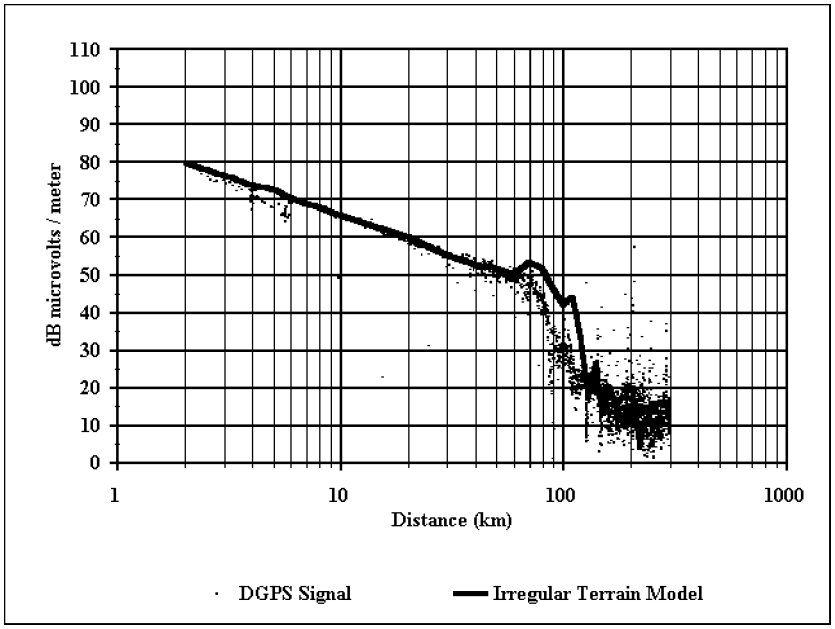

Figure 48. Comparison of measured and predicted field strength vs. distance going west from the FAA beacon at Bennett, Colorado - irregular terrain.

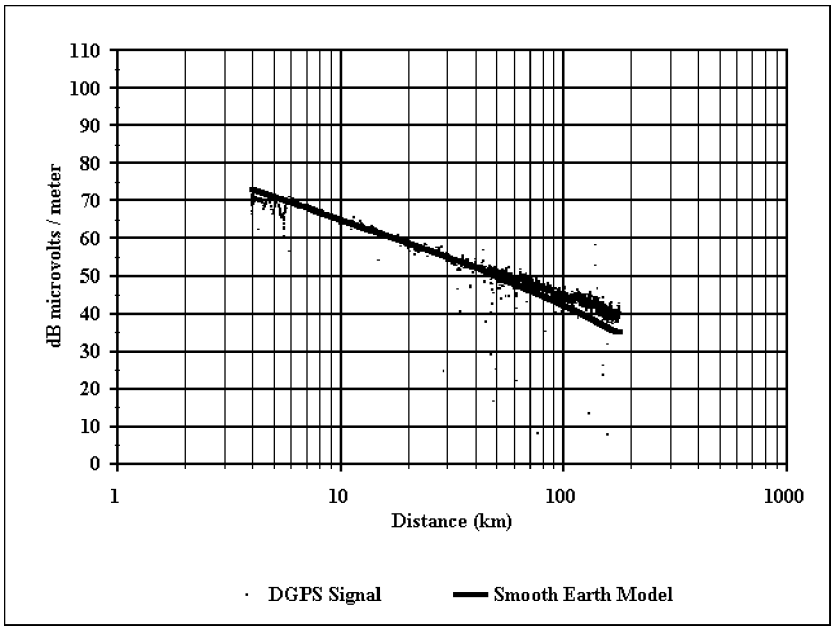

Figure 49. Comparison of measured and predicted field strength vs. distance going north from the FAA beacon at Bennett, Colorado - smooth earth.

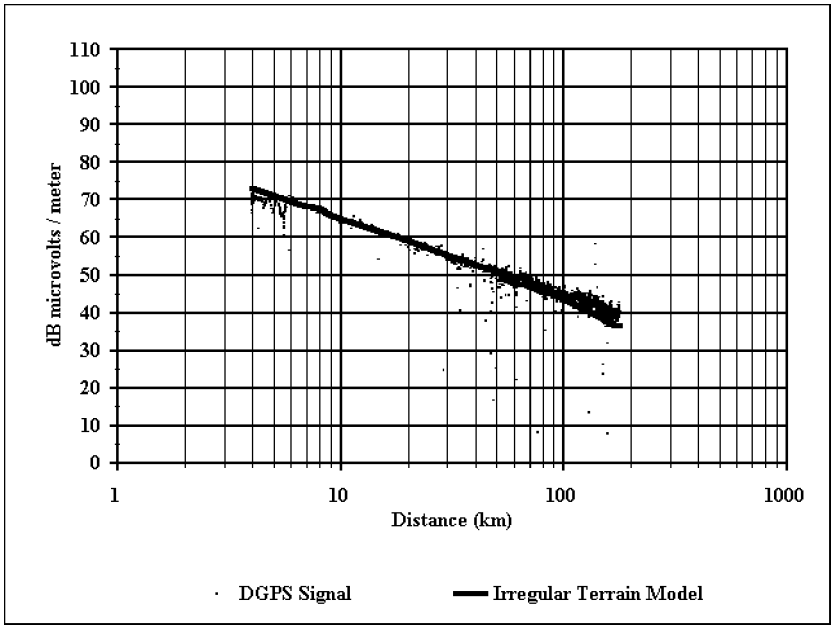

Figure 50. Comparison of measured and predicted field strength vs. distance going north from the FAA beacon at Bennett, Colorado - irregular terrain.

10. ACKNOWLEDGMENT

The authors wish to thank James A. Arnold of the Federal Highway Administration, Department of Transportation for funding this work.

11. REFERENCES

[1] W.J. Dixon, and F.J. Massey, *Introduction to Statistical Analysis*, New York: McGraw-Hill, Inc., 1969, pp. 345-347.

[2] E. Haakinson, S. Rothschild, and B. Bedford, "MF broadcasting system performance model," NTIA Report 88-237, Aug. 1988.

[3] N. DeMinco, "Ground-wave analysis model for MF broadcast systems," NTIA Report 86-203, Sep. 1996.

[4] K. Furutsu, R.E. Wilkerson, and R.F. Hartmann, "Some numerical results based on the theory of radio wave propagation over inhomogeneous earth," *Radio Science* 68D, No. 7, pp. 827-846, Jul. 1964.

APPENDIX A: SIGNAL FIELD STRENGTH COMPUTATIONS

Field strength is measured in dBμV/m as seen by the receiving antenna. This is calculated from the peak-power value and the antenna-correction factor using the following equations:

$$G_{dB_i} = -29.79 + 20\log_{10}(f_{MHz}) - ACF, \tag{A1}$$

where G_{dB_i} is the gain of the antenna in dBi, f_{mHz} is the frequency in MHz, and *ACF* is the antenna correction factor in dB;

$$A = \frac{\lambda^2 * 10^{\frac{G_{dB_i}}{10}}}{4\pi}, \tag{A2}$$

where *A* is the aperture of the antenna in units of m^2, and λ is the wavelength of the carrier frequency in meters;

$$\lambda = \frac{c}{f_{Hz}}, \tag{A3}$$

where *c* is the speed of light in m/s (3e8 m/s), and f_{Hz} is the carrier frequency in Hz;

$$P_d = \frac{P_{m(watts)}}{A}, \tag{A4}$$

where P_d is the power density in watts/m^2, and $P_{m(watts)}$ is the power in watts measured at the output of the antenna;

$$E_{dB(\frac{\mu v}{m})} = 20 * \log_{10}(1e6 * \sqrt{P_d * 377}), \tag{A5}$$

where $E_{dB(\frac{\mu v}{m})}$ is the E field in dBμV/m measured at the antenna, and 377 is the impedance of free space measured in ohms.

APPENDIX B: NOISE FIGURE AND SENSITIVITY COMPUTATIONS

For a multistage amplifier that has stage power gains G_1, G_3, G_3,… (linear form), and stage noise figures F_1, F_3, F_3,… (linear form), respectively, the overall noise figure is [1]

$$F = F_1 + \left[\frac{(F_2 - 1)}{G_1}\right] + \left[\frac{(F_3 - 1)}{G_1 G_2}\right] + \cdots \tag{B1}$$

The measurement system seen in Figure 9, has a single stage gain of 22.4 dB (Mini-Circuits amplifier) with a typical noise figure of 2.9 dB. Cable losses and the insertion loss of the low pass filter are negligible. The noise figure of the spectrum analyzer is 31 dB. From Equation (B1), the overall noise figure of the system is 9.6 dB.

The bandwidth and overall noise figure of the system determine the smallest signal that can be detected; it is computed from the following equation:

$$NP = -174 + 10\log_{10}(B) + F_{dB}\,, \tag{B2}$$

where *NP* is the noise power in dBm, -174 is the thermal noise in a 1-Hz bandwidth at room temperature (300° K), *B* is the bandwidth of the system in Hz, and F_{dB} is the overall noise figure of the system in dB. The quantity *NP* is the minimum signal power that can be detected at the output of the antenna. In this case, the bandwidth of the system is 300 Hz. Therefore, using Equation (B2), *NP* is calculated to be -139.6 dBm, or expressed in watts,

$$NP = \frac{10^{\left[\frac{-139.6}{10}\right]}}{1e3} = 10.96e-18\,. \tag{B3}$$

Knowing *NP*, one can calculate the sensitivity of the system at the input to the antenna using Equations (A1) through (A5) (see Appendix A). Assuming a typical carrier frequency of 300 kHz and the corresponding antenna-correction factor of 40.5 dB, the minimum power density at the input to the antenna must be 16.18e-15 watts/m^2 in order to be detected. This corresponds to a field strength of 7.85 dB μv/m.

REFERENCE

[1] F.G. Stremler, *Introduction to Communication Systems*, Reading, Massachusetts: Addison-Wesley Publishing Company, 1997, pp. 173-174.

APPENDIX C: CORRECTION FACTORS FOR THE EATON 94592-1 ANTENNA

Table C-1 lists the antenna correction factors for the Eaton 94592-1 monopole antenna used during measurements. The antenna was measured to an absolute accuracy of 2 dB.

Table C-1. Antenna Correction Factors

Frequency (kHz)	Antenna Correction Factor (dB)
285.0	41.2
287.0	41.2
289.0	41.0
291.0	40.9
293.0	40.9
295.0	40.7
297.0	40.7
299.0	40.6
301.0	40.5
303.0	40.5
305.0	40.4
307.0	40.4
309.0	40.4
311.0	40.4
313.0	40.2
315.0	40.1
317.0	40.1
319.0	40.1
321.0	40.0
323.0	39.9
325.0	39.9

APPENDIX D: COMPUTATION OF EXPECTED ELECTRIC FIELD STRENGTH

For a known power into a transmitting antenna and a given antenna efficiency, the expected signal strength in dB μV/m can be determined at a specified distance from the transmitter. Assuming the signal is radiating isotropically into a hemisphere (see Figure D-1), the power is evenly distributed over a surface equal to $2\pi r^2$ (where r is the distance from the transmitter in meters). The power density at the receiver expressed in watts/m^2 can be determined by

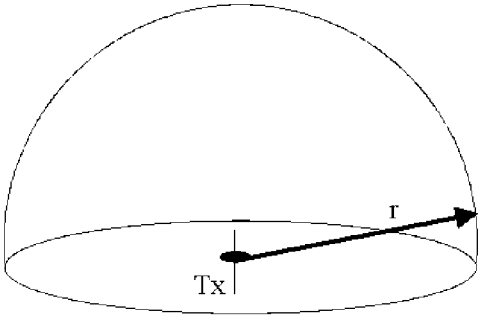

Figure D-1. Signal radiating isotropically into a hemisphere.

$$P_d = \frac{P_t e}{2\pi r^2}, \quad \text{(D1)}$$

where e is the efficiency of the transmitting antenna and P_t is the input power.

The electric field E in dB μV/m is determined by

$$E = 20 \log_{10}(1\text{e}6 \sqrt{P_d 377}), \quad \text{(D2)}$$

where 377 is the impedance of free space measured in ohms.

As an example, a transmitter with an antenna efficiency e between 15 and 20% and signal power P_t into the antenna of 1000 W, the expected power density P_d at 10 km would be between 238.7e-9 and 318.3e-9 watts/m^2 (Equation D1). The expected electric field strength E at the same distance is between 79.5 and 80.8 dB μV/m (Equation D2).